IR and Raman Spectroscopies Probing MOFs Structure, Defectivity, and Reactivity

IR and Raman spectroscopies probing MOFs structure, defectivity and reactivity

Francesca Bonino,[1] Carlo Lamberti,[1,2] and Silvia Bordiga,[1,*]

[1] Department of Chemistry, NIS and INSTM Reference Centers, University of Torino, Via Quarello 15, I-10135 Torino, Torino, Italy.
[2] Southern Federal University, Zorge Street 5, 344090 Rostov-on-Don, Russia

1. Introduction

Vibrational spectroscopies, mainly infrared but to some extent also Raman, have been among the most informative techniques in understanding the structure and the reactivity of surface species present in high surface area materials such as oxides, zeolites and, more recently, MOFs.[1-18] In the specific case of MOFs, the peculiar sensitivity of vibrational techniques to different chemical groups allows to verify the presence/absence of the solvent phase, to identify the nature of the linkers, to determine the successful insertion of functional groups, and to evidence the possible presence of structural defects in the framework. Section 2 is devoted to the discussion of such aspects showing how the technique is able to check the quality of the synthesis products.

The possible presence of coordination vacancies at the metal center created after the desolvation can be investigated using appropriate probe molecules and measuring the probe-surface interaction via the perturbation inferred to the probe by the adsorption sites. The observables are the changes in vibrational frequency and intensity of the probe modes. IR-inactive modes can also be observed as a result of the interaction with the surface. In MOFs it is also possible to follow induced changes of skeletal and surfaces modes of the framework. Such information is of crucial relevance for applications such as gas adsorption, separation and storage, and pertinent examples are reported in Section 3.

Finally, Section 4 describes how the use of infrared is able to monitor catalytic reactions inside MOFs. Summarizing, this brief review work is aimed to underline, with pertinent specific examples, how IR and Raman can contribute to a better understanding of MOFs structure, properties and reactivity.

2. Raman and IR spectroscopy to check the synthesis product

2.1 Identification of defects in UiO-66

In the case of UiO-66 synthesis,[19] there is a lack of understanding of how the product is affected by changes in synthesis parameters. There are several ways in which a given UiO-66 sample may

differ from the idealized, nondefective material of composition $Zr_6O_4(OH)_4(BDC)_6$.[20,21] The most dramatic way that a sample may deviate from ideality is that it may have a significantly lower thermal stability than expected. In ref.[22] a systematic study, demonstrating the dramatic yet logical impact that the synthesis conditions can have on the properties of UiO-66, is reported. It has been found that, above all others, a method previously employed by Serre and co-workers[23] reproducibly yields a robust product with high thermal stability. Two features of this procedure stand out: (1) the use of 220 °C as the synthesis temperature and (2) an excess of BDC is added such that the BDC:Zr molar ratio in solution is 2:1. This differs from most other synthesis procedures in which the synthesis temperature is typically limited to 90−120 °C and BDC is added to the synthesis mixture in a 1:1 stoichiometric ratio with Zr.[19]

With the aim of elucidating why the former method produces a superior UiO-66 product, a systematic series of samples, in which three different synthesis temperatures (100, 160, and 220 °C) and five different BDC:Zr ratios (1:1, 5:4, 3:2, 7:4, and 2:1) were used, have been synthesized and then characterized. Moreover, the effect of DMF washing and methanol exchange procedures has been assessed. Samples were labeled by the formula "UiO-66-x-L:M-y" where x = synthesis temperature, L:M = BDC:Zr ratio, and y describes the extent of washing (blank = unwashed, 2DMF = washed twice in DMF, MeOH = methanol exchanged after two DMF washes).[22]

Figure 1 compares the Raman spectra recorded on the samples at the two extremities of the series (grey curve: UiO-66-100-1:1-MeOH; red curve: UiO-66-220-2:1-MeOH) with that simulated[24] from a model of the ideal UiO-66 structure (green curve).

The close resemblance of the simulated Raman spectrum to that experimentally collected on UiO-66-220-2:1-MeOH is conspicuous, a finding which not only emphasizes the ideality of the sample, but also allows the synergistic power of the experimental/computational approach to be demonstrated. That is, the complete Raman spectrum of UiO-66-220-2:1 can now be assigned irrefutably by visualization of the relevant vibrational modes on the idealized model. Note that this is only possible due to the near equivalence of the experimental and simulated data. The full assignment is presented in ref. [22], where the web address link (http://www.crystal.unito.it/vibs/uio66_hydro/)[25,26] to visualize the vibrational modes of UiO-66 may via animations is also given.

In Figure 1, it can be seen that the spectrum of UiO-66-100-1:1 (grey curves) clearly deviates from the model. Several discrepancies are observed, with the most severe being accentuated by asterisks. To this end, the model once again proves useful in that it tells us that the two asterisked regions (appearing at ca. 1450 and 870 cm^{-1}) are associated with carboxylate based and O-H bending modes respectively. Carboxylate based modes are exactly those one would expect to be most affected by linker deficiencies. The observation of peculiarities in this region therefore provides compelling further evidence for the presence of missing linker defects on this sample. Of further note is the distinct lack of bands below 500 cm^{-1} in the spectrum of this material, a region where several bands are expected to appear. The majority of the bands in this portion of the spectrum are associated with vibrations involving the Zr-O bonds of the inorganic cornerstones. The absence of these bands suggests that either the cornerstone vibrations are strongly affected by linker deficiencies or there are defects on the clusters themselves.

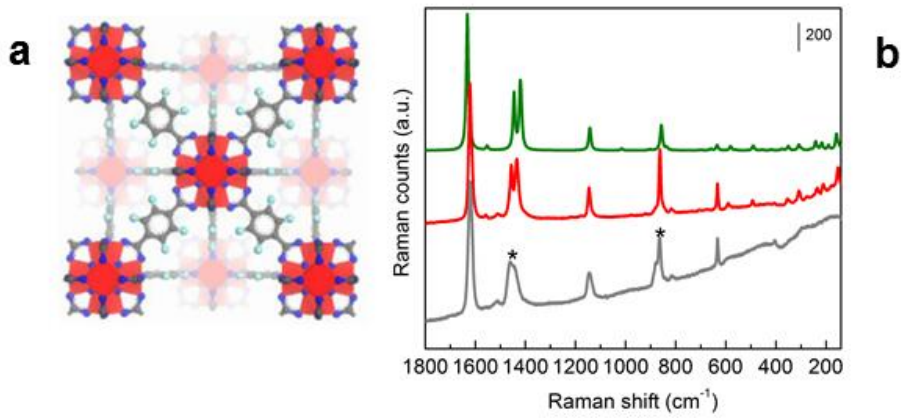

Figure 1. Part a: Representation of the 3D structure of the UiO-66 with 1,4-benzene-dicarboxylate (BDC) as linker. **Part b**: Raman spectra simulated from a model of the ideal UiO-66 structure (green curve), measured on UiO-66-220-2:1-MeOH (red curve), measured on UiO-66-100-1:1-MeOH (grey curve); before measurement, the samples were activated at 150 °C for 2h under vacuum. Spectral regions which deviate significantly from the model spectrum are marked by asterisks.[Part a: adapted from adapted from Ref.[19] with permission, copyright ACS 2008; Part b: adapted from Ref.[22] with permission, copyright ACS 2014]

2.2. Identification of Lewis acidity as possible defects in MIL-140 MOFs

Recently, Serre et al.[27] reported the synthesis of porous zirconium dicarboxylate MOFs based on the reactions of $ZrCl_4$ with 1,4-H_2BDC (1,4-benzenedicarboxylic acid), 2,6-H_2NDC (2,6-naphthalenedicarboxylic acid), 4,4'-H_2BPDC (4,4'-biphenyldicarboxylic acid), and H_2Cl_2ABDC (3,3'-dichloro-4,4'-azobenzenedicarboxylic acid). A whole series of porous zirconium dicarboxylate solids, denoted MIL-140A to MIL-140D, with a general formula $[ZrO(O_2CR\text{-}CO_2)]$ (R=C_6H_4 (MIL-140A), $C_{10}H_6$ (B), $C_{12}H_8$ (C), $C_{12}N_2H_6Cl_2$ (D)) has been isolated and characterized, and their properties compared with those of the polymorphs UiO-66 and its upper analogues.[27]

These solids all have the same *c* parameter (ca. 7.8 Å), consistent with the inorganic subunit of complex zirconium oxide chains, oriented along the *c* axis (see Figure 2), connected to six other chains through the dicarboxylate linkers. This delimits triangular channels along the *c* axis. The zirconium atoms exhibit a seven coordination mode with three μ_3-O oxygen atoms and four oxygen atoms from the dicarboxylate groups. Inorganic chains can be considered either as resulting from the linkage of two parallel corner-sharing chains or chains of edge-sharing dimers of zirconium polyhedra.

Unlike the UiO series (formulated as $[Zr_6O_4(OH)_4(O_2C\text{-}R\text{-}CO_2)_6]$,[19,28] no structural hydroxy groups but only minor amounts of coordinated water were identified by IR spectroscopy on the MIL-140s. This composition was reflected by the lack of any Brønsted acidity in the in vacuum activated materials.

In the 150-200°C range under vacuum DMF was removed first; adsorbed water (band around 1639 cm^{-1}) and acid (band in the 1730-1740 cm^{-1} range) were fully removed at 250 °C under vacuum resulting in materials free of any impurities. All the MOFs remained stable under vacuum up to 350°C at least (see Figure 2b and c). The region corresponding to the hydroxyl groups is shown in Figure 2d. Before activation or after heating under vacuum at moderate temperature, a broad band was observed at 3639 cm^{-1} on MIL-140A, MIL-140B and MIL-140C and at 3619 cm^{-1} on MIL-140D. Another large perturbation around 3300 cm^{-1} may also be observed indicative of H-bonding perturbation which starts decreasing upon evacuation. These bands disappeared completely after activation at 300°C. The bands around 3600 cm^{-1} are broader than those found for the structural hydroxyls on UiO-66. In addition, it is noteworthy that their intensity decreased at the same time as the band at 1638 cm^{-1}. This suggests that the bands around 3600 cm^{-1} rather belong to coordinated water. On MIL-140A and C, a very weak and sharp band is observed at 3673 cm^{-1} which might be indicative of a low amount of hydroxyls probably present on defective sites. Conversely Lewis acid sites were

detected by the presence of an adsorption band characteristic of coordinated CD_3CN species (ν(CN) mode at 2300 cm^{-1}). This band is at the same position for all the MIL-140 solids, which implies a similar acid strength. However, the intensity of the band, hence the amount of Lewis acid sites detected by CD_3CN, varies from one solid to the other (see Figure 2e).

While comparable for MIL-140A and C, the concentration of Lewis acid sites is highest for MIL-140D, however MIL-140A,C, and D have similar values when expressed in amount of sites per m^2 of surface area. Noteworthy, the amount of Lewis sites on MIL-140D represents one tenth of the Zr atoms which compares well with the values obtained for UiO-66 (see Figure 2f).

The presence of Lewis acid sites could be tentatively attributed to acidic sites on the external surface. However, this is unlikely, as pyridine, which is not expected to enter the pores of MIL-140A, should be adsorbed just as well on the external surface, which is not the case. Only a very small amount of sites was detected for MIL-140B, which was further confirmed by both pyridine and CO adsorption at 77 K. Nevertheless, the low amount of coordinately unsaturated sites (less than 10% of the Zr atoms) precludes their identification by PXRD. These Lewis acid sites could originate from 1) the dehydration of coordinated species, such as for UiO-66, 2) the presence of defects, or 3) a local change in the coordination mode of the Zr atoms upon adsorption of species. Thermogravimetric analysis (TGA) and IR spectroscopy were therefore used to qualitatively assess the hydrophobic character of these solids.

MIL-140s can be considered as rare examples of slightly hydrophobic porous solids that have a significant amount of Lewis acid sites. Besides, these materials revealed a high hydrothermal and a good mechanical stability. This paves the way for their use for applications, such as catalysis, adsorption, or separation.

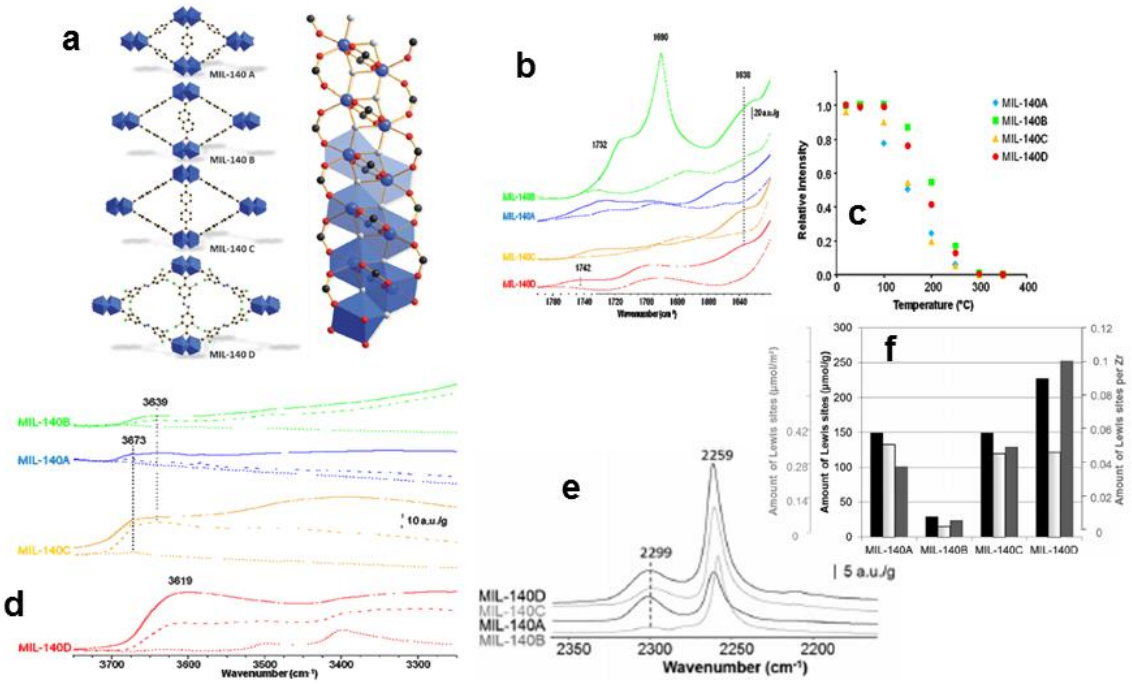

Figure 2. Part a: left, view of the crystal structure for the series of MIL-140(Zr) solids along the *c* axis; right: view of the inorganic subunit of MIL-140, Zr atoms or polyhedra blue, C black, and Cl green, O atoms from the linker are red and oxo groups are gray. **Part b**: FTIR spectra on the MIL-140 solids, after heating at 50°C (full lines) and 300°C (dashed lines). **Part c**: Relative intensity determined by FTIR spectra of remaining free acid on the MIL-140 solids after thermal treatment. **Part d**: FTIR spectra on the MIL-140 solids, after heating under vacuum at 50°C (full lines), 150°C (intermediate) and 300°C (dashed lines). **Part e**: Acidity of the MIL-140s determined by CD_3CN adsorption monitored by FTIR spectroscopy. **Part f**: density of Lewis acid sites, based on the mass of the solid (black bars; left scale), to its BET surface area (light gray bars; outer left scale), or to the number of Zr atoms (dark gray bars; right scale). [Adapted with permission from Ref. [27], copyright Wiley VCH 2012].

2.3 Evaluation of functionalization effect in mixed-ligand UiO-66 MOFs

A series of mixed-ligand [1,4-benzenedicarboxylic acid (BDC)/2-amino-1,4-benzenedicarboxylic acid (ABDC)] UiO-66 metal–organic frameworks (MOFs), synthesized through two different methods (low (LT) and high temperature (HT)) and having NH_2 content ranging from 0 to 100% (see Figure 1a) have been studied by focusing the attention on the CO_2 adsorption performance.[29,30]

For the two series of samples, preliminary FTIR studies on the best activation temperature (in vacuo) were performed. In particular, the aim was to identify the minimum temperature at which all residual solvent (H_2O and traces of DMF) could be removed, while preserving the majority of the structural hydroxyl groups on the LT/HT UiO-66 samples. All other samples were then subjected to the same treatment. The required activation conditions were different, depending on the synthesis method used: 393 K for 2 h for the LT samples and 423 K for 1 h for the HT samples. The FTIR spectra recorded on activated LT- and HT-ML-MOFs are reported in Figure 3b1 and 3b2, respectively. A very intense band 3673 cm^{-1} can be observed in all spectra; this was previously assigned to hydroxyl groups on the inorganic cornerstones of the materials.[31] The intensity of this band is observed to decrease with increasing 2-amino-1,4-benzenedicarboxylic acid (ABDC) content, as clearly shown in the inset of Figure 3b1, in which the spectra obtained for LT-UiO-66 and LT-UiO-66-NH_2 are compared. Focusing attention on the spectra recorded on the LT-MLMOFs (Figure 3b1), the intensity of the asymmetric and symmetric NH stretching bands, appearing at 3518 and 3404 cm^{-1}, respectively, can be clearly seen to systematically increase with the amino content of the samples. These two bands are blue-shifted with respect to those observed on the free ABDC ligand (3508 and 3393 cm^{-1}).[32] This means that the NH_2 groups in the MOFs undergo hydrogen bonding to a lesser extent than those in pure ABDC. Interestingly, a shoulder at 3328 cm^{-1} is only clearly visible on the spectra recorded on the LT-ML-MOF series of samples. At lower (1800–900 cm^{-1} range) vibrational frequencies, the spectra of the amino-modified materials show additional bands with respect to the unfunctionalized material at 1707, 1656, 1628, 1339, and 1254 cm^{-1} (close to the range of OCO carboxylate asymmetric and symmetric stretching modes, 1650–1350 cm^{-1})[31] and at 1127 and 968 cm^{-1}. Some of these bands feature in the FTIR spectrum simulated from the model UiO-66-NH_2-50 structure (see Figure 3c).

The intensity of all of these bands increases in proportion to the amino content of the samples. Conversely, the very sharp and intense band at 1019 cm^{-1} is progressively eroded with increasing amino content. This band is assigned to one of the benzene ring CH deformation modes and is particularly active when the NH_2 functionality is absent.[31] Diffuse reflectance infrared Fourier transform (DRIFT) results previously reported by Chavan et al.[29] confirm some of these observations.

The same qualitative changes to the MOF spectra with NH_2 content are also observed for the HT-ML-MOFs (Figure 3b2). However, the NH_2 stretching bands appear at the lower frequencies of 3495 and 3387 cm^{-1}, respectively, such that they are red-shifted with respect to the free ABDC linker. Furthermore, the full-width at half maximum (FWHM) increases such that observation of the low-frequency shoulder is obscured. At frequencies higher than those of the carboxylate OCO stretching modes (1650–1350 cm^{-1}),[31] only a single shouldering band is present, whereas, at lower frequencies, bands centered at 1339, 1254, 1127, and 968 cm^{-1} are observed. Erosion of the benzene ring CH deformation band at 1019 cm^{-1} is also observed in this HT-ML-MOF series.

The IR spectrum simulated from an idealized model of UiO-66-NH2-50 is reported in Figure 3c and shows good agreement with that of LT-UiO-66-NH2-57. In the NH stretching region, two peaks are clearly observed, due to asymmetric and symmetric vibrations of NH_2 functional groups. For a better comparison between the computed and experimental IR spectra, an estimated anharmonic correction of 150 and 122 cm^{-1} was applied to the OH and NH stretching modes, respectively, while frequencies in the 3300-1000 cm^{-1} range were uniformly scaled by a factor 0.98. In addition, a larger FHWH

(Full Width at Half Maximum) was used for the NH stretching modes to take into account the broadening of the corresponding peaks due to the H-bonding interaction of the NH_2 group with the oxygen of the carboxylate.

The resulting simulated spectrum nicely agrees with that obtained experimentally. The OH and NH stretching regions fit particularly well with the model, such that a semi-quantitative agreement is observed, allowing the three bands to be unambiguously assigned to one OH stretch and two NH stretching modes. In addition, computed data confirm that the peak around 1019 cm^{-1} is characterized by modes due to the C-H deformation of the linkers without the amino groups, as for UiO-66, while the new bands around 1050 and 980 cm^{-1} are CH deformations coupled with NH modes in the ABDC linkers. It turns out that the intensity of the band at 1019 cm^{-1} decreases as observed experimentally.

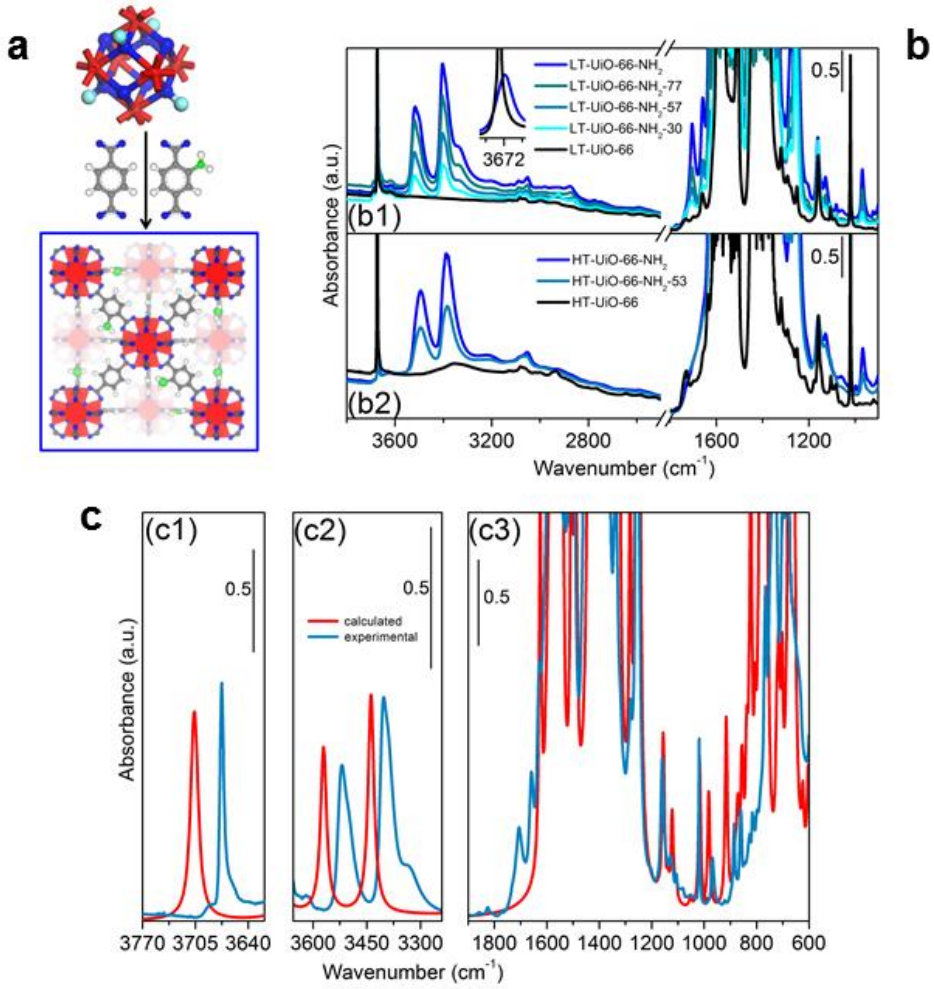

Figure 3. **Part a**: 3D model of the structure of mixed-ligand [1,4-benzenedicarboxylic acid (BDC)/2-amino-1,4-benzenedicarboxylic acid (ABDC)] UiO-66 metal–organic frameworks (MOFs). **Part b**: FTIR spectra of activated a) LT-ML-MOFs and b) HT-ML-MOFs. **Part c**: Simulated (red) and experimental (light blue) FTIR spectra of hydroxylated UiO-66-NH2-50 and LT-UiO-66-NH_2-57, respectively. The spectra are divided into three regions: c1) the OH stretching region; c2) the NH_2 stretching region; and c3) the framework mode region. [Figure adapted from Ref. [30], copyright Wiley VCH 2014]

3. Spectroscopic monitoring of gas adsorption

Surfaces of MOFs can show very peculiar properties in respect of small molecules (gases of vapor phases) being characterized by a large varieties of sites that can interact with them in many ways[15]. On one side, vibrational spectroscopies (IR and in few cases Raman) of probe molecules adsorption, were used to clarify the acidity of Bronsted sites,[28,31,33] or the accessibility of Lewis sites (metal centers with coordinative unsaturation) in respect to different probe molecules.[34-39] On the other

side, variable temperature infrared spectroscopy,[40,41] allowed to evaluate thermodynamic parameters of the adsorption phenomena (ΔH and ΔS), giving valuable information on these materials in respect of their properties as adsorbers, for gas separation, or for gas capture and storage.[42-45]
Extensive work has been published to describe major aspects of infrared spectroscopy of molecular hydrogen adsorbed on a large variety of MOF topologies and on a well characterized homologue set of samples having the same topology and different cations inside.[46],[47] In order to find practical application as selective adsorbents towards gases relevant to the energy field, an even larger set of data was obtained for M_2(dobdc) materials (dobdc^{4-} = 2,5-dioxidobenzene-1,4-dicarboxylate).[48],[49] In this case the focus was carbon monoxide (Section 3.1) where the spectroscopic data were combined with structural and volumetric insights,[45] and on carbon dioxide (Section 3.2).

3.1 Carbon monoxide adsorbed in M_2(dobdc)

Carbon monoxide is one of the most commonly used molecular probe as it is very sensible and quite specific, as its way to interact with metal cations, involves different contributions, according to the nature of the metal-cations sites. Spectroscopically, CO molecule undergoes an upwards shift (blue-shift) of its stretching frequency, with respect to the gas (2143 cm^{-1}), when it interacts with point charges (such as an alkaline earth metal cation)[50-52] or in presence of an acceptor of electron pairs (such as a metal cation acting as Lewis acidic center).[53] In the former case, the electric field created by a positive charge causes a polarization of the CO molecule proportional to the local electric field of the site,[51] owing to the increase of the force constant of the C–O bond. In the latter case, the presence of an acceptor of electron pairs the C-end lone pair of CO is transferred to the metal cation giving rise to a σ-coordination ($M^{n+} \leftarrow$ CO).[13,54,55] It is generally accepted that the higher the blue-shift, the stronger the interaction is.
When transition metal ions are involved, the interaction of CO can lead to a more complex situation due to both electrostatic and chemical type interaction. Chemical type interaction involves both ligand-to-metal σ donation (from the full 5σ orbital of CO to the empty d_z^2 orbital of the metal) with concomitant metal-to-ligand (from a full d_{xz} orbital of the metal to the empty $2\pi^*$ of CO) back donation. In these cases, adducts are also formed at room temperature and the sign of the $\Delta\tilde{\nu}$ (CO) shift, will depend on the extent of contribution of both type of interactions.[7,10,13,55,56]
A nice example is shown in Figure 4 where, background subtracted FTIR spectra of CO (20 mbar) adsorbed on M_2(dobdc) collected during the progressive lowering of CO coverage (where M was Zn, Mg, Mn, Fe, Co, Ni respectively) are illustrated.[45] For the sake of simplicity, spectra obtained at high CO coverage (showing rotovibrational contribution of gaseous CO) are removed. In addition, the spectral evolution (grey curves) at intermediate CO coverages is reported only for Ni and Zn samples.
The main IR absorption bands in the six materials are observed at: 2173(Zn), 2178 (Mg), 2172 (Mn), 2160 (Fe), 2164 (Co) and 2178 (Ni) cm^{-1} and were assigned to the stretching vibration of CO in the $M^{2+}\cdots$CO adducts. In all the samples these main band are blue shifted with respect to the free CO molecule. In case of Mg_2(dobdc), Mg^{2+} ions lack d electrons and are thus unable to back-donate into the empty CO π* orbitals. Moreover, the empty Mg 3d levels are too high in energy to be engaged for σ donation from the lone pair electrons of CO. The Mg^{2+}−CO interaction is thus primarily electrostatic in nature, inducing an increase of the C−O stretching frequency [43], giving rise to the highest-energy infrared stretch of the series (2178 cm^{-1}, consistent with those reported for CO adsorption in Mg^{2+}-exchanged zeolites.[57]). Zn^{2+} ions in Zn_2(dobdc), having a fully occupied set of 3d orbitals, are not available to accept σ donation from CO, resulting in a similarly high infrared stretch of 2173 cm^{-1}. An equivalent behaviour is observed in the case of Mn_2(dobdc), in which the ν(CO) of 2172 cm^{-1} is red-shifted with respect to Mg_2(dobdc), as a result of diminished polarization by the larger-radius, softer Mn^{2+} ions and presumably only a very small, nearly negligible π

backbonding contribution. The metal ions in both Fe_2(dobdc) and Co_2(dobdc) are smaller and more polarizing than Mn^{2+}; however, the C−O stretching frequencies displayed by these materials (2160 cm^{-1} for Fe^{2+} and 2164 cm^{-1} for Co^{2+}) are the lowest reported here, suggesting slightly more pronounced π interactions. Finally, Ni_2(dobdc) displays the highest CO stretching frequency among the transition metal cations (2178 cm^{-1}), since Ni^{2+} is the smallest and most polarizing ion [37]. Given the small, charge-dense nature of Ni^{2+}, its lower energy π-type 3d orbitals are less well-suited for back-donation into CO than either Fe^{2+} or Co^{2+}.

Upon progressive increase of P_{CO}, some relevant changes are observed. The main peak grows in intensity, broadens and shifts to lower frequency (in this conditions it is not possible to determine exact maxima; as most of the bands go out of scale). This behavior suggests that high occupancy of M^{2+} sites requires structure rearrangement with the formation of slightly different adducts characterized by new energetic minima, as confirmed by isosteric heats of CO adsorption calculated from isotherms measured at 298, 308, and 318 K [45].

In general, CO adsorbed at the M^{2+} sites in M_2(dobdc) shows rather smaller shift in wavenumber when compared with CO adsorbed at respective cations inside zeolites.[58-62] The high frequency shift in case of zeolites has been explained by considering the combination of high number of coordination vacancies and the strong electrophilic nature of the cations. However, these shifts are large when compared with CO adsorbed on 5-fold coordinated sites in the respective oxides (MgO, CoO, and NiO +14, -7 and +9 cm^{-1} respectively).[7,41] The lower shift in oxides was explained by considering purely electrostatic interaction for MgO and contribution of π-back donation for CoO and NiO in terms of the Madelung effects generated by an almost infinite alternation of cations and anions present on oxides surfaces.[63-66] Very particular is the CO adsorbed on ZnO[63] which shows absorption peak at 2190 cm^{-1} which is at higher wavenumber than that of CO adsorbed on Zn_2(dobdc). This high shift in CO vibrational frequency on ZnO, can be explained by considering strong electrophilic nature of 3-fold coordinated Zn^{2+} sites in ZnO.[67] Concurrently, the growth of some minor bands on both the low (2130-2100 cm^{-1}) and high frequency side (2230-2180 cm^{-1}) of the main bands is observed in all samples. At lower frequency, complex absorptions in the range 2129-2120 and 2115-2110 cm^{-1} have been assigned to the stretching mode of ^{13}CO in M_{5c}^{2+}–^{13}CO adducts and to a $M^{2+}\cdot\cdot O^{12}C$ species respectively. Bands observed at higher frequencies (2230-2180 cm^{-1} interval), with respect to the main components already discussed, can be argumentatively assigned to the combination modes of the ν(CO) mode with phononic bands involving M^{2+} sites. This explains the quite large interval in frequencies, recalling the large spread of values observed in case of the main band. Finally, at high CO coverage (spectra reported only in case of Zn and Ni samples, grey curves) the presence of liquefied CO inside the pores is evidenced by the appearance of a band at 2135 cm^{-1}.[68,69]

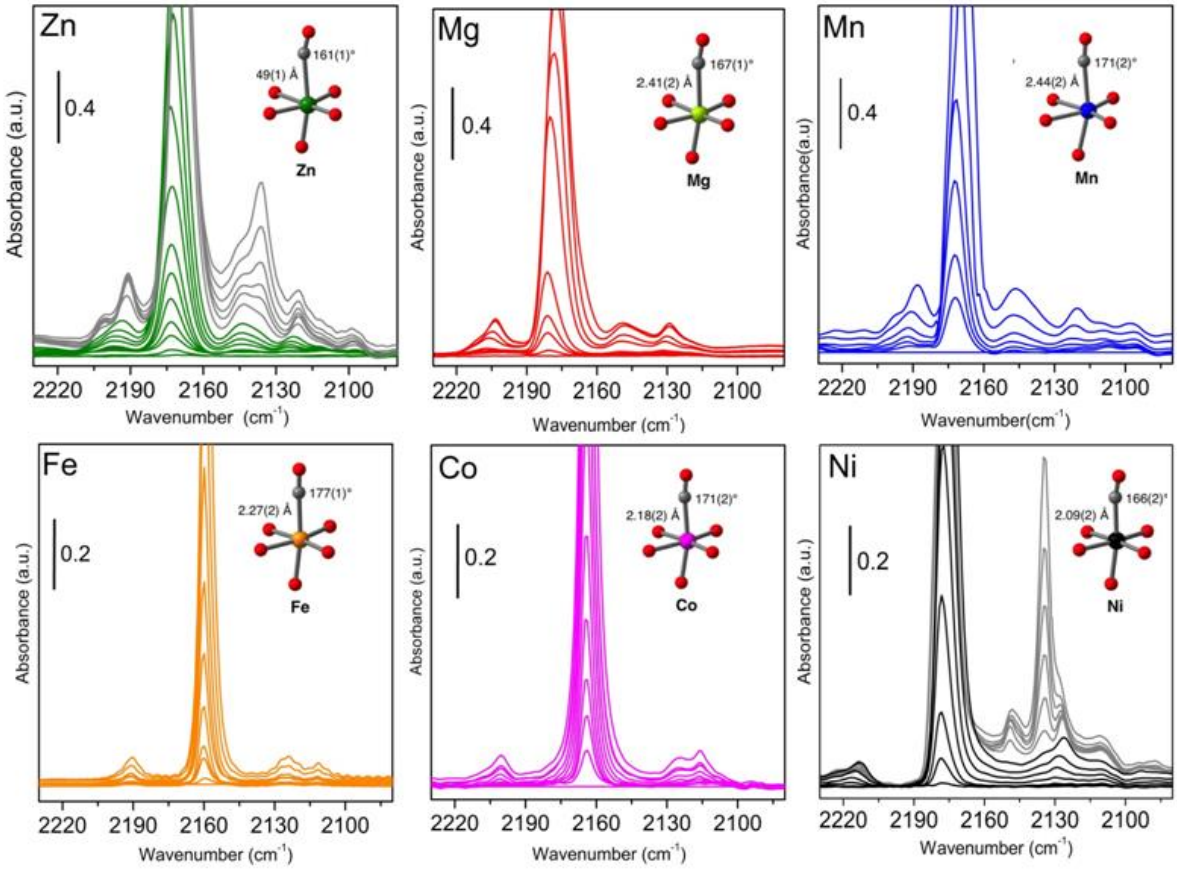

Figure 4. Background subtracted FTIR spectra, at liquid nitrogen temperature, of decreasing CO coverages on M_2(dobdc) pre-activated at 180 °C for 2h in high vacuo (see labels in each panel) The corresponding first coordination sphere for the M^{2+} ions in M_2(dobdc)·1.5CO, with M−CO distances and M−C−O angles are indicated in each panel (data obtained from Rietveld analysis of powder neutron diffraction data). [Adapted with permission from Ref. [45], copyright ACS 2014.]

The stability of Ni-CO adduct allowed also to obtain a Raman spectrum of this species.[36] Figure 5 compares Raman spectrum of the outgassed sample with that obtained in presence of 60 mbar of CO (spectra collected at the temperature of the laser beam). In the ν(CO) frequency range (inset of Figure 5) a single band centered around 2175 cm^{-1} is present.[36] It can be easily ascribed to ν(CO) of $Ni^{2+}\cdots CO$ adducts formed inside the CPO-27-Ni upon high CO dosage. The much simpler Raman spectrum, in respect of the infrared one, is due to the fact that in Raman only the most stable species can be detected (temperature effects) and, moreover, is associated to the fact that Raman spectroscopy works in scattering mode, monitoring a much smaller portion of sample, in respect to the Infrared performed in transmission mode. Much weaker signals in the skeletal mode region (1700-1000 cm^{-1}) allow to follow the perturbing effect of CO with respect to specific vibrations of the materials. It is relevant to observe that some bands are strongly perturbed by CO adsorption, while some other are left unchanged. In particular the bands at 1625 and 586 cm^{-1}, assigned to benzene ring vibrations, shift to 1616 and 575 cm^{-1}, respectively; the bands at 1427 and 833 cm^{-1}, due to $\nu(COO)_{sym}$ and δ(CH), move to 1410 and 824 cm^{-1} and the ν(Ni–O) band at 430 cm^{-1} is shifted at 419 cm^{-1}. Surprisingly, in case of Raman spectrum, no bands show a blue shift upon CO interaction, as it has been observed in case of the IR spectrum.

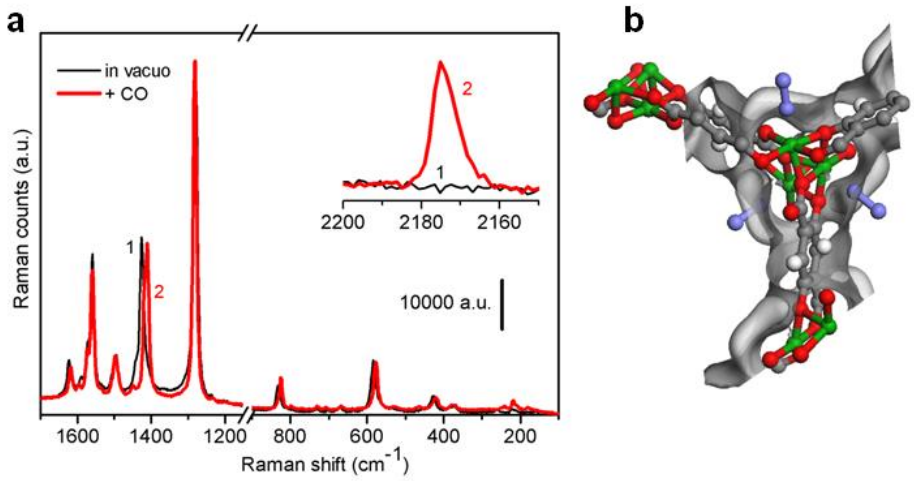

Figure 5. Part a: room temperature Raman spectra of Ni_2(dobdc) outgassed at 393 K for 1 h before (black curve 1) and after (red curve 2) CO adsorption (60 mbar). The main part reports the framework vibration perturbed by CO adsorption, the inset shows the ν(CO) stretching region. Part b: Graphic representation of CO coordination sites. [Adapted with permission from Ref.[36], copyright ACS, 2009.]

Both infrared and Raman spectra show a blue-shift in the ν(CO) stretching frequency coordinated to the cations, consistent with non classical metal-CO interactions involving little or no π back-donation.[13,54,55] Along the series, spectroscopic differences have been evidenced and found agreement in structural determinations and energetic evaluations. Structure determinations from powder neutron diffraction data reveal M–CO distances ranging from 2.09(2) Å for M = Ni to 2.49(1) Å for M = Zn and M–C–O angles ranging from 161.2(7)° for M = Mg to 176.9(6)° for M = Fe. Electronic structure calculations applying density functional theory (DFT) were in good agreement with the trends apparent in the infrared spectra and crystal structures only in case of fully relaxed extended framework structure upon CO binding. Adsorption isotherms collected at 298, 308, and 318 K indicate reversible adsorption, with capacities for the Fe, Co, and Ni frameworks approaching one CO per metal cation site at 1 bar (about 6.0 mmol/g and 157 cm^3/cm^3). The six frameworks display (negative) isosteric heats of CO adsorption ranging from 52.7 to 27.2 kJ/mol along the series Ni > Co > Fe > Mg > Mn > Zn, in good agreement with the results of DFT calculations. The reversible CO binding at high capacity and moderate energy suggests that these frameworks may be of utility for the separation of CO from various industrial gas mixtures, including CO/H_2 and CO/N_2. Selectivities determined from gas adsorption isotherm data using ideal adsorbed solution theory (IAST) over a range of gas compositions at 1 bar and 298 K indicate that all six M_2(dobdc) frameworks could potentially find application as solid adsorbents to replace current cryogenic distillation technologies, with the choice of M dictating adsorbent regeneration energy and the level of purity of the resulting gases.[45]

3.2 Spectroscopic monitoring of carbon dioxide adsorption

Carbon dioxide is widely used as a probe molecule to monitor both acid and basic sites, as those found in metal oxides or zeolites.[70-72]. CO_2 belongs to the $D_{\infty h}$ symmetry group and has four fundamental modes: the symmetric stretching ν_1, the doubly degenerate bending vibration ν_2, and the asymmetric stretching vibration ν_3. For symmetry reasons, the ν_2 and ν_3 modes are infrared active, whereas ν_1 is only Raman active. In the free molecule, these modes appear at 1388.3 (ν_1), 667.3 (ν_2), and 2349.3 (ν_3) cm^{-1}. Adsorption may cause the lowering of molecular symmetry which results appearance of Raman active mode in IR spectra. The presence of strong acid - base pair at the surface may result in chemical reaction of CO_2 and carbonated and bicarbonate are formed, which are characterized by IR absorption in the 1700-1400 cm^{-1} frequency range. In case of alkaline and

alkaline earth metals exchanged zeolites, e.g. for Mg-ETS-10, the formation of carbonates has been evinced by a doublet at 1620 and 1380 cm^{-1}.[72]
Despite to what observed in case of nucleophilic metal centers (because of high electron density given by a charge or by the presence of electron donating ligands) that bind the weakly electrophilic CO_2 molecule through carbon,[73] CO_2 interacts with cations (Lewis centers), through one of the oxygen lone pair orbitals with formation of weak end-on adducts.[71] The formation of these species (linear $M^{x+}\ldots O=C=O$ adduct causes a small perturbation of the ν_3 mode (asymmetric O=C=O stretching).
As previously made in case of zeolites, infrared spectroscopy has been used, in combination with other techniques, to describe the nature of the interaction of carbon dioxide with respect to some metallorganic framework investigated to develop new adsorbents for CCS, trying to describe the nature of the adducts both formed with cations and or with Brønsted sites.[43,74-77]
Figure 6 shows the FTIR spectra obtained for decreasing CO_2 equilibrium pressure (from grey to blue) at room temperature on -Mg, -Co and -Ni –(dobdc) (part a b and c respectively). FTIR spectra obtained for CO_2 adsorption on all three structural analogues are characterised mainly by the ν_3 stretching, doubly degenerate bending mode (ν_2) and $\nu_3+\nu_1$ and $\nu_3+2\nu_2$ in Fermi resonances modes of CO_2 adsorbed in end on configuration forming $M^{2+}\cdots O=C=O$ adducts.
The ν_3 stretching mode of the $^{13}CO_2$, which is present naturally in $^{12}CO_2$ (1%) is also observed on the low frequency side of the main absorptions. In M_2(dobdc), the strong absorptions associated to the carboxylate modes of the framework avoid any spectral inspection in the range 1600-1300 cm^{-1} however, as no appreciable change has been observed where the asymmetric mode of the carbonate is expected (1620 cm^{-1}), this allows to exclude the formation of these species. The perturbation in CO_2 upon adsorption cause the shift of the stretching and bending modes, that lose their degeneracy and appear as doublets (observed frequencies and assignments are listed in Table 1). As in all cases only polarisation effect can be taken into account, it is strange to observe ν_3 stretching mode blue shifted on –Mg, and red shifted on –Co and –Ni homologues. The splitting of bending mode degeneracy on –Mg, –Co and –Ni and distorted CO_2 structure found Ni_2(dobdc), demonstrate the strong interaction of CO_2 with open metal sites in M_2(dobdc) framework. In the high frequency region (3800-3500 cm^{-1}), two components are observed. The nature of these two absorptions is well known and is interpreted on the basis of combination of ν_1 and ν_3 modes of CO_2. The reason for the presence of a doublet shifted of about ± 50 cm^{-1} from the expected frequency for the combination mode ν_1 and ν_3, is due to the fact that the first overtone of ν_2 mode coincides with the ν_1 mode, causing a strong Fermi resonance effect that induces a band splitting in two components 100 cm^{-1} apart.

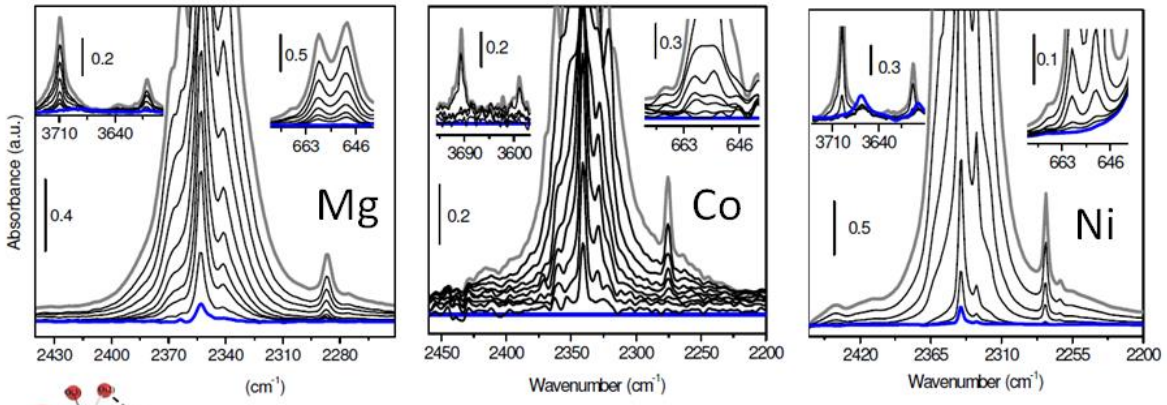

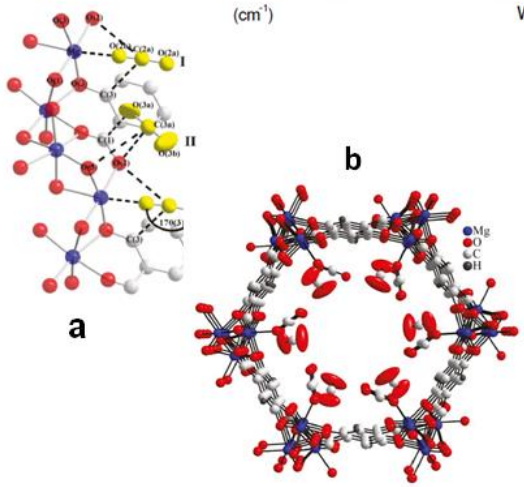

	Mg	Co	Ni
M...O(CO_2) (Å)	2.27(1)	2.23(4)	2.29(3) *
O–C–O(CO_2) (°)	178(2)	174(4)	162(3) *
M–O–C(CO2) (°)	131(1)	118(2)	117(2) *
$-Q_{st}$ (kJ mol^{-1})	43.5(2)	33.6(1)	38.6(6)

Figure 6 Top: FTIR spectra of CO_2 adsorbed on M_2(dobdc) (Mg, Co and Ni, from left to right respectively) at decreasing equilibrium pressure (higher coverage grey curve correspond to 0.02 atm equilibrium pressure). Insets report the bending right) and $\nu_3+\nu_1$ and $\nu_3+2\nu_2$ Fermi resonance mode of the CO_2 (left). Reproduced with permission from Ref. [78]. **Bottom:** Structures obtained through Rietveld refinement of neutron powder diffraction data on Mg_2(dobdc). **Part a)**: Close up view of Mg-MOF-74 loaded with 1.75 CO_2 (yellow) per Mg showing the nearest neighbour interactions found between the CO_2 sites (I and II) and the framework. These are shown as dashed black lines. **Part b)** Ball and stick model of Mg_2(dobdc) loaded with 1.75 CO_2 per Mg. The thermal ellipsoids are drawn at 50% probability. **Parts a and b** are reproduced with permission from Ref.[79], copyright ACS 2011. Data reported in the table are taken from [80] apart from those marked with * (taken from [75]).

Upon increasing the equilibrium pressure the bands associated to combination modes of ν_1 and ν_3 become very intense and shift indicating the filling of the cages. The shift in these components and broadening of the ν_3 mode of the $M^{2+}\cdots CO_2$ can be associated with the contribution of physisorbed CO_2 which cause a change in dielectric constant. The spectroscopic data can be explained only with an end-on coordination of CO_2 and a slight bending of the CO_2 molecule, as observed by XRD, was hypothesized. A bending can be explained by considering the steric and electronic environment around the coordinated carbon dioxide. Especially, the short C5⋯O1 interaction of 3.00(3) Å may indicate a secondary interaction between the framework O5 atom and the C atom of CO_2, leading to a slight bending in a similar manner as previously suggested to take place in zeolites[71] and in HKUST-1.[74]

Table 1. Vibrational frequencies of bending ν_2 , stretching ν_3 and $\nu_3+\nu_1$ and $\nu_3+2\nu_2$ Fermi resonance mode of $^{12}CO_2$ and ν_3 of $^{13}CO_2$ adsorbed on M_2(dobdc) (M=Mg, Co and Ni)

	Vibrations				
Material	$\nu_2(CO_2)$ (cm^{-1})	$\nu_3(CO_2)$ (cm^{-1})	$\nu_3(^{13}CO_2)$ (cm^{-1})	$\nu_3+\nu_1$ (cm^{-1})	$\nu_3+2\nu_2$ (cm^{-1})
CO_2 Gas	667.3	2349	2283		
Mg_2(dobdc)	649, 658	2353	2287	3599	3709
Co_2(dobdc)	654, 659	2341	2275	3590	3696
Ni_2(dobdc)	651, 659	2342	2276	3588	3696

Structural study of CO_2 adsorption was performed the first time on Ni_2(dobdc),[75] showing that CO_2 molecule was clearly coordinating the Ni^{2+} atom in the framework end-on through one of its oxygen atoms, with a Ni^{2+}–O distance of 2.30(2) Å and a Ni-O-C angle of 117(2)º. The resulting CO_2 species found slightly distorted from its usual linear structure with an O-C-O angle of 162(3) °. This last result was revisited more recently in a comprehensive work devoted to compare the full series of M_2(dobdc) interacting with CO_2 in term of their structural properties and gas adsorption behaviour.[80] High resolution neutron powder diffraction (NPD) experiments showed that intramolecular angles of CO_2 molecules adsorbed at the metal cations exhibit minimal deviations from 180 °, lending more awareness of the framework properties required to achieve CO_2 activation, information that is pertinent to ongoing discussions regarding chemical conversion of CO_2. Moreover, these structural studies, combined with volumetric measurements, revealed that secondary CO_2 adsorption sites, while likely stabilized by the population of the primary adsorption sites, significantly contribute to adsorption behaviour at ambient temperature (see Figure 6). Low-coverage CO_2 isosteric heats of adsorption for the M_2(dobdc) analogues (calculated at a loading of 0.1 CO_2 per M^{2+}) were found in good agreement with theoretical values obtained with density functional theory calculations including van der Waals dispersion contributions and considering comparable loadings (quantum zero-point energies (ZPEs) and finite-temperature thermal energies (TEs) at the level of a harmonic approximation, were also considered).[80] All these findings contributed to complete some previous studies that were considering a single material[43,75] or that were focusing the attention mostly to their adsorption behaviour.[81-83]

Breathing MOF frameworks,[84,85] such as those referring to the MIL-53 topology, suggested to follow their behaviour with respect to carbon dioxide adsorption in a wide range of equilibrium pressure (1-10 bar)[77,86] also along the collection of infrared spectra. Figure 7 summarizes the results obtained by following "in situ" IR spectra evolution upon CO_2 adsorption from 1 to 10 bar to the activated sample and then progressive decrease of the equilibrium coverage. An evaluation of adsorbed CO_2 amount was estimated from the integrated intensity of the ν_2 CO_2 bands between 645 and 665 cm^{-1} (5b). Adsorption–desorption profiles deduced from the evolution of the intensities of these peaks versus pressure (Figure 7b, top) are similar to those reported from microcalorimetry experiments. The splitting of ν_2 mode of CO_2 into two maxima testifies a lowering in symmetry of adsorbed CO_2 molecule. In the high CO_2 pressure range (from 5 to 10 bar), a new ν_2 band appeared at 659 cm^{-1} (Fig. 5b). This band is persistent during the desorption process down to 2–3 bar CO_2, which was the pressure that corresponded to the closing of the structure at the end of the hysteresis loop. Moreover it is evident that the framework responds to the interaction with CO_2, as testified by the pronounced shift of ν18a ring mode associated to the terephthalate entities that moves from 1022 to 1017 cm^{-1} at high pressure. Also in this case adsorption–desorption profiles deduced from the evolution of the intensities of these peaks versus pressure, showed a remarkable hysteresis loop Figure 7a, top.

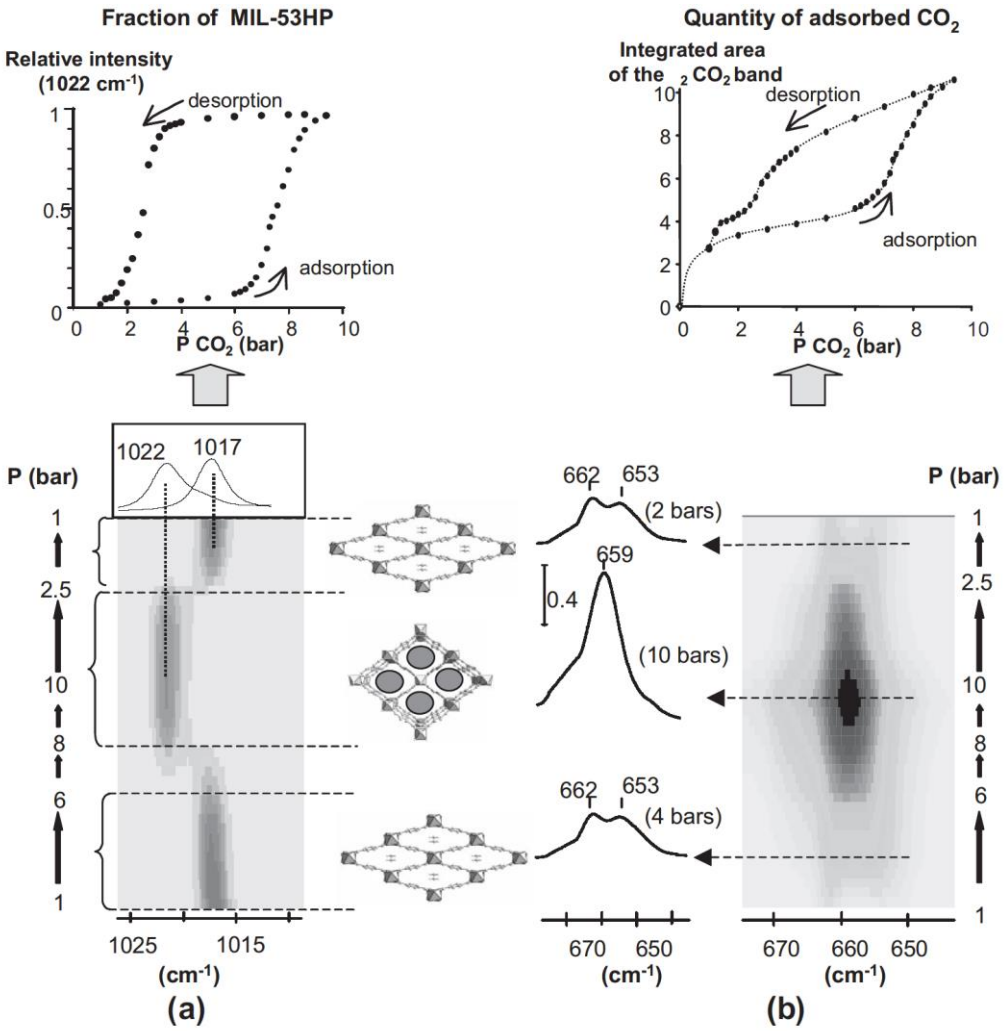

Figure 7. Bottom (2D IR Map): a) Variation in the intensities of MIL-53LP (1017 cm^{-1}) and MIL-53HP (1022 cm^{-1}) bands and b) in the ν_2 CO_2 bands (653, 662 cm^{-1} MIL-53LP; 659 cm^{-1} MIL-53HP versus CO_2 pressure. Top: hysteresis phenomenon observed during an adsorption–desorption cycle. Curves were obtained from the quantitative analysis of the corresponding IR spectra. [Reproduced with permission from Ref.[77], copyright Wiley VCH 2007.]

As final example about how infrared can monitor under "operando" conditions the interaction of CO_2 with a MOF, we want to report some fascinating results where, in a series of post synthesis aliphatic amine modified MOFs, resulted in a strong interaction of CO_2 upon adsorption and desorption[87] giving rise to the reversible formation of carbamate species. In particular, the attachment of alkyldiamines to coordinatively unsaturated metal sites accessible inside the pores of some metal-organic frameworks, has been demonstrated a good strategy to get high activity and selectivity towards low pressure CO_2 adsorption.[88-90] Most notably, functionalization of Mg_2(dobpdc) (dobpdc^{4-} = 4,4′-dioxidobiphenyl-3,3′-dicarboxylate), an expanded variant of the well-studied metal-organic framework Mg_2(dobdc), with N,N′-dimethylethylenediamine (mmen) generated an adsorbent with exceptional CO_2 capacity under flue gas conditions and unusual step-shaped adsorption isotherms that make it superior to other solid or liquid sorbents for the efficient capture of CO_2.[90] Spectroscopic and structural studies (Powder X-ray diffraction data performed on the isostructural compound mmen-Mn_2(dobpdc)) allowed to fully describe the interaction mechanism of CO_2, along the charge and discharge profile. As described in part b of Figure 8, simultaneous proton transfer and nucleophilic attack of N on a CO_2 molecule forms an ammonium carbamate species that destabilizes the amine coordinated at the next metal site, initiating the cooperative adsorption of CO_2 by a chain

reaction. Thus, the adsorption of CO_2 at ambient temperatures is associated with a structural transition to form an extended chain structure held together by ion pairing between the metal-bound carbamate units and the outstretched ammonium group of a neighbouring mmen molecule. Infrared spectroscopy measurements performed on mmen-Mg_2(dobpdc) fully support the proposed mechanism.

As shown in Figure 8 (black curve), upon activation of mmen-Mg_2(dobpdc), two distinct N–H vibrations at 3330 and 3255 cm^{-1}, attributable to N_f and N_c of mmen, are clearly discernable. Upon exposure to CO_2, the simultaneous disappearance of both N–H resonances indicates that while the mmen to CO_2 stoichiometry is one-to-one, the amine to CO_2 stoichiometry follows the expected two-to-one stoichiometry. Moreover a deep change in the ν(C-H) of the amine (3000 - 2750 cm^{-1}) testifies a strong perturbation occurred upon CO_2 adsorption. Interaction with CO_2 at 150°C leads to the appearance of a band at 1690 cm^{-1} ascribable as ν(C=O) of random pairs of ammonium carbamate (see part b of Figure 8). This feature does not change in intensity over the whole investigated temperature range; conversely two new bands at 1330 and 658 cm^{-1} ascribable as ν(C-N) and [β(OCO) + β(NCO)] only appear in correspondence of the phase-change transitions, being characteristic of the high order structured carbamate species. As observed by infrared spectroscopy, while CO_2 can reversibly adsorb under all conditions via the formation of non-ordered ammonium carbamate pairs, appropriate temperature and pressure conditions allow CO_2 to rearrange into a highly specific orientation, and it is this process that endows these materials with their unique adsorption properties.

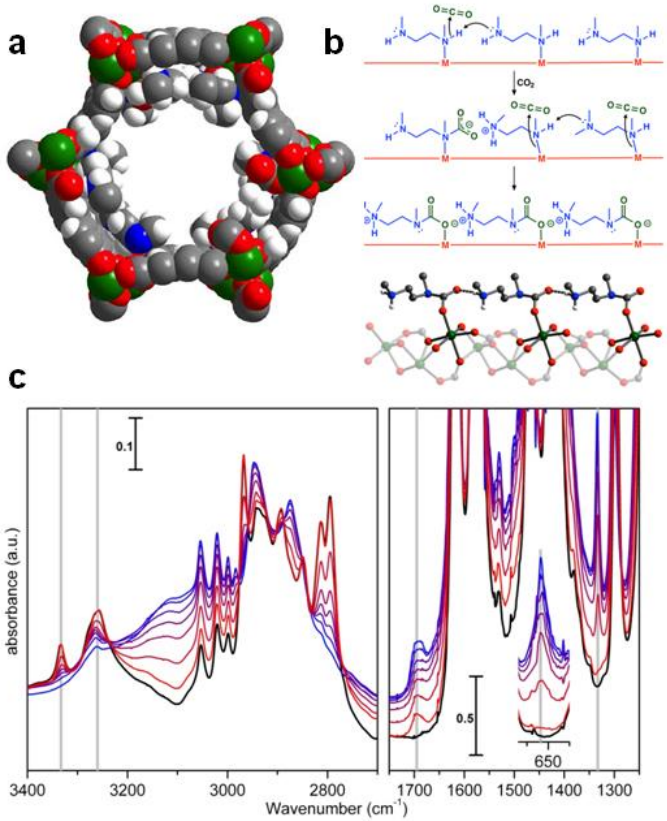

Figure 8. **Part a**: Graphical model of CO_2-mmen-M_2(dobpdc). Green, gray, red, blue, and white spheres represent M, C, O, N and H atoms, respectively. **Part b:** Depiction of the mechanism for CO_2 adsorption at four neighbouring M–mmen sites within an infinite one-dimensional chain of such sites running along the crystallographic c axis of a mmen-M_2(dobpdc) compound. Simultaneous proton transfer and nucleophilic attack of N on a CO_2 molecule forms an ammonium carbamate species that destabilizes the amine coordinated at the next metal site, initiating the cooperative adsorption of CO_2 by a chain reaction. **Part c** FTIR spectra changes of mmen-Mg_2(dobpdc) upon interaction with 5% CO_2 in N_2 at different temperatures, from 150°C (red curve) to 30°C (blue curve). For sake of comparisons activated sample is also reported (black curve). Major bands are underlined by grey lines. [Adapted with permission from Ref. [87], copyright Nature publishing group 2014.]

4. Spectroscopic monitoring of catalytic reactions

4.1 Fe_2(dobdc) catalyst in presence of N_2O

Enzymatic haem and non-haem high-valent iron–oxo species are known to activate strong C–H bonds, yet duplicating this reactivity in a synthetic system remains a formidable challenge. Although instability of the terminal iron–oxo moiety is perhaps the foremost obstacle, steric and electronic factors also limit the activity of previously reported mononuclear iron(IV)–oxo compounds. These challenges may be mitigated within metal–organic frameworks that feature site-isolated iron centers in a constrained, weak-field ligand environment.

Fe_2(dobdc), also known as Fe-MOF-74 or CPO-27-Fe, possess the hexagonal channels of the framework lined with a single type of square pyramidal iron(II) site (see Figure 9a). Its reactivity towards nitrous oxide, a gaseous two-electron oxidant and O atom transfer agent that is widely employed in industry, anticipating the generation of a highly reactive iron(IV)–oxo species capable of oxidizing strong C–H bonds.

It has been shown that Fe_2(dobdc) ($dobdc^{4-}$ = 2,5-dioxido-1,4-benzenedicarboxylate) is able to activate the strong C–H bonds of ethane and convert it into ethanol and acetaldehyde using nitrous oxide as the terminal oxidant.[91] In the absence of a hydrocarbon substrate, the Fe(IV)–oxo quickly decays via hydrogen-atom abstraction into an Fe(III)–hydroxide, which is isolable and well characterized. This hydroxide species can react with weak C–H bonds, such as those in 1,4-cyclohexadiene, to form benzene and H_2O-bound Fe_2(dobdc).

To establish the coordination mode of N_2O in Fe_2(dobdc), powder neutron diffraction data, which are very sensitive to the atomic assignment of O and N, were collected on a sample dosed with various loadings of N_2O. At low loadings, the best fit was an average of approximately 60% η^1-O and 40% η^1-N coordination, with Fe–N_2O distances of 2.42(3) and 2.39(3) Å, respectively. In both cases, a bent Fe–N_2O angle close to 120° was observed (see Figure 9a).

FTIR spectroscopy revealed to be very useful in characterizing both the Fe(II)-N_2O adduct and the subsequentely formed, Fe(III)–hydroxide active species. Contact with 40 mbar of N_2O causes the appearance of extremely strong bands in the 2280–2160 cm^{-1} spectral range, associated with ν(N–N) of N_2O, while the rest of the IR spectrum is substantially unaffected (see blue curve in Figure 9b). Dominant absorptions due to the framework modes below 1600 cm^{-1} does not allow the monitoring of the ν(N–O) band in N_2O, expected to be around 1286 cm^{-1}. The spectrum profile testifies the formation of a condensed phase inside the Fe_2(dobdc) channels, as the ν(N–N) does not present the expected profile of a free linear rotator (P and R branches with the lack of the pure vibrational transition, Q branch). The spectrum at highest coverage (blue curve) is characterized by a very intense band, ascribable to the ν(N–N) in N_2O molecule, behaving as an hindered rotator. The maximum is observed at 2226 cm^{-1}, a position very close to that expected for the fundamental transition of pure N_2O molecule (2224 cm^{-1}). The very small blue shift with respect to the position of N_2O gas allows us to assert that N_2O interacts weakly with the Fe(II) species, giving rise to a physically adsorbed (liquid-like) phase. The main peak is accompanied by further components at higher (clear maximum at 2240 cm^{-1}) and lower (broad features at 2220, 2214 and 2206 cm^{-1}) frequencies, suggesting that, at the measuring temperature (beam temperature), N_2O molecule still partially maintains its roto-vibrational profile. In case of Fe-silicalite the appearance of a doublet at 2282 cm^{-1} and at 2248 cm^{-1} was assigned to the formation of two slightly different Fe–N_2O adducts, while a component at 2226 cm^{-1} was associated to the formation of weaker adducts with Brønsted sites.[92] In the present case similar assignments are discarded, as all the above-mentioned signals disappear at the same rate upon outgassing at room temperature. The total reversibility of these components further confirms the weak nature of the interaction of N_2O with the Fe(II) sites in Fe_2(dobdc) sample.

Prolonged heating in N_2O at 60 °C gives rise to a spectrum characterized by a strong band at 3678 cm^{-1} and by a clear component at 670 cm^{-1} (see green curve in Figure 9b). The peak at 3678 cm^{-1} can be associated to the ν(O–H) and the component at 670 cm^{-1} can be ascribed to the ν(Fe–OH) (see

inset b1 in Figure 9). The formation of these hydroxide species is associated to the reactivity of N_2O, as testified by the intensity decrease of the band due to adsorbed N_2O (see inset b2 in Figure 9).
CO titration experiments before and after heating Fe_2(dobdc) in the presence of N_2O were performed (see Figure 9c) and the intensity of the band centered at 2160 cm^{-1} (vibrational mode of CO interacting with Fe(II) in Fe_2(dobdc)[45]) was considered for evaluating the fraction of remaining Fe(II) unsaturated sites, that resulted to be less than 10%.

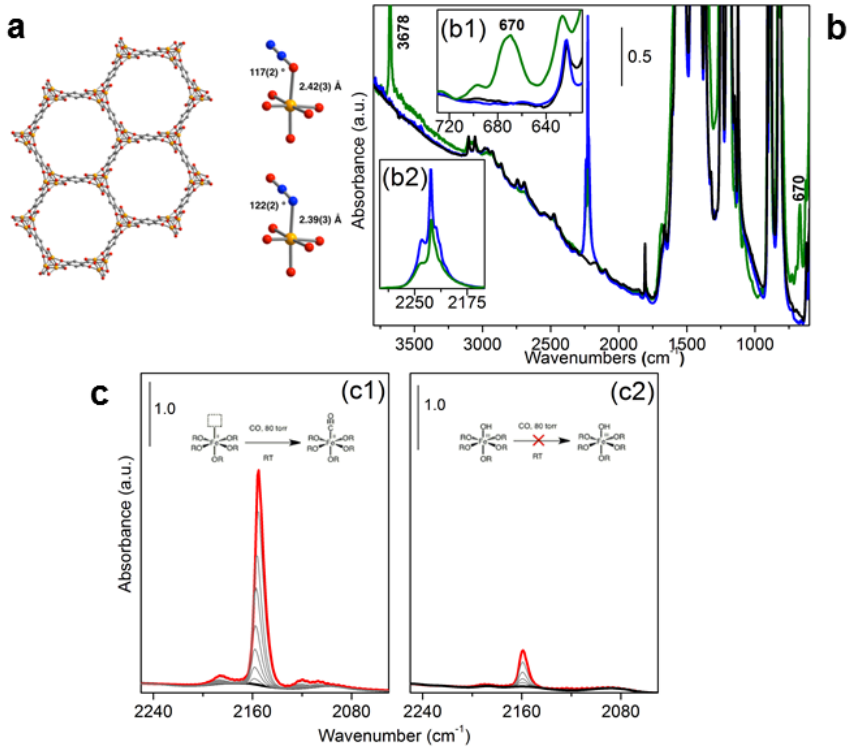

Figure 9. Part a: Structure of Fe_2(dobdc), showing hexagonal channels lined with five-coordinate iron(II) sites, and experimental structures for N_2O binding in Fe_2(dobdc), solved from powder neutron diffraction data collected at 10 K. Orange, grey, dark blue and red spheres represent Fe, C, N and O, respectively; H atoms are omitted for clarity. **Part b**: a thin film of Fe_2(dobdc) was activated at 433 K for 18 h (black curve), in contact with 180 mbar of N_2O at room temperature (blue curve) and heated at 60 °C for 14 hours (green curve). Inset (b1): magnification of 730–610 cm^{-1} spectral range, testifying the formation of $Fe_2(OH)_2$(dobdc). Inset (b2): background subtracted spectra illustrating the ν(N–N) region. **Part c**: CO dosed on an activated sample of bare Fe_2(dobdc) (c1) and CO dosed on a sample that has been contacted by N_2O overnight at 60 °C (c2). [Adapted with permission from Ref.[91], copyright Nature publishing group 2014.]

4.2 Cr-MIL-101 encapsulated Keggin phosphotungstic acid as active nanomaterial for catalysis.
Cr-based MIL-101 (Materials of the Institut Lavoisier no. 101) is a mesoporous MOF reported by Férey and co-workers.[93] MIL-101(Cr) is constructed from linkage of 1,4-benzenedicarboxylate (H_2BDC) anions and inorganic trimeric Cr building units leading to a three-dimensional cubic structure of corner-sharing supertetrahedra. MIL-101 has mesosize cages of 2.9 and 3.4 nm, accessible through microporous windows of 1.2 and 1.45 nm, giving rise to a high Langmuir surface area of 5900 $m^2\ g^{-1}$ (see Figure 10a).
MIL-101(Cr) encapsulated Keggin phosphotungstic acid (HPW) [MIL-101(HPW)] was demonstrated to be an active heterogeneous catalyst for selective catalysis of the ring opening reaction of styrene oxide with methanol, achieving 99% yield of 2-methoxy-2-phenylethanol in 20 minutes at 40 °C. Similar MIL-101 samples prepared using one-pot microwave synthesis in the absence of HPW or in the presence of hydrofluoric acid (HF) were less active.
The impact of fluoride and HPW polyanion incorporation on the acidity of MIL-101 was investigated by the in situ infrared spectroscopy technique using CO as a probe molecule. Additional hydroxyl

groups and Lewis acid sites are present in MIL-101(HPW) explaining the observed superior catalytic performance in styrene oxide methanolysis. The Keggin polyanion has a relatively large particle size of ca. 1.3 nm diameter and 2.25 nm^3 in volume. Five Keggin ions take up a 10.1 nm^3 volume, which is approximately 50% of the total volume of a large cage (20.6 nm^3) as reported by Férey and co-workers.[93]

The incorporation of Keggin HPW in MIL-101 was confirmed by IR spectroscopy based on the characteristic bands at 822, 903 ν(W–O–W), 983 ν(W=O) and 1084 cm^{-1} ν(P–O) (see Figure 10b, black spectrum).[93] Of course all MIL-101 spectroscopic fingerprints in the 1200–700 cm^{-1} range are also present. The highest frequency range (3850–2500 cm^{-1}, see inset a1) shows again many similarities between the MIL-101(H_2O) and MIL-101(HPW) samples. These IR spectra were recorded on samples activated at 200 °C to remove all residual solvent and physisorbed water. In this spectral range a lot of bands are due to combination and overtone modes. Nevertheless, some fingerprints are clearly distinguishable: the bands at 3070 cm^{-1} and 3592 cm^{-1} due to ν(C–H) aromatic linker stretching vibration and to ν(O–H) stretching mode, respectively. The presence of an OH group is to compensate for the negative default charge per trimer of chromium octahedra.

The catalytic activity of three considered MIL-101 samples in ring opening of styrene oxide is in the following order: MIL-101(H_2O) < MIL-101(HF) < MIL-101(HPW). This trend evidenced the need to further investigate the catalytic sites of the three different MIL-101 catalysts by means of in situ IR spectroscopy and using CO as a probe molecule known to be a very sensitive probe (see Figure 10c).[36,39,44,45] In all the three samples, already at room temperature, a quite intense and sharp band is always present at 2194 cm^{-1} (light green spectra) showing the presence of strong Cr^{3+} exposed Lewis sites. By lowering the temperature with liquid nitrogen, the band increases in intensity and shifts to 2197 cm^{-1} (dark green spectra).[94] In parallel at lower frequency, bands due to CO physisorbed (liquid-like) species arise (main feature cantered at 2135 cm^{-1}). Besides these features in common with the other two samples, MIL-101(HPW) shows a broadening of the band cantered at 2197 cm^{-1}. In particular, when at low temperature CO coverage is decreased, a further component centered at 2202 cm^{-1} clearly appears. The assignment is not straightforward, but we can hypothesize the presence of other Lewis sites, different from the Cr^{3+} environment present in MIL-101(H_2O) and MIL-101(HF) samples. Two possible new species can be proposed: (i) some defects in encapsulated polyanion forming new Lewis sites or (ii) Cr^{3+} sites with different acidity because of the presence of HPW. The CO probing study revealed that the presence of the fluoride ion has no significant Lewis acidity enhancement effect in MIL-101(HF). Interestingly, in styrene oxide methanolysis MIL-101(HF) was more active than MIL-101(H_2O).

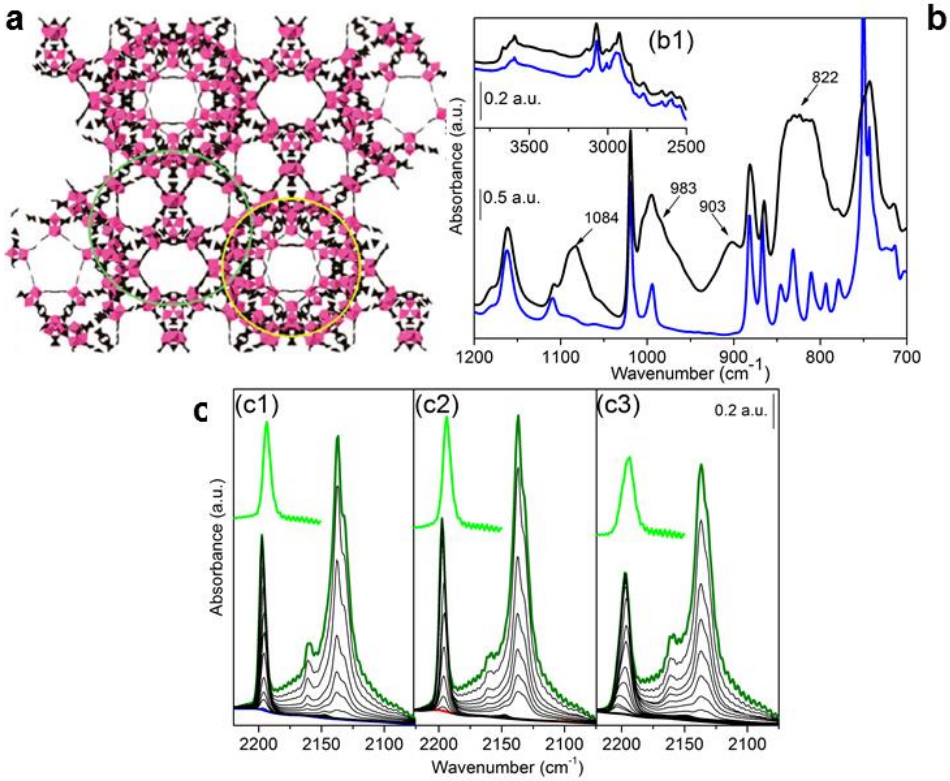

Figure 10. Part a: MIL-101 crystal structure with the boundary of the large cage highlighted green and that of the small cage highlighted yellow. The Cr polyhedrons are colored pink. **Part b**: IR spectra collected after outgassing at 200 °C of MIL-101(H_2O) (blue) and (b) MIL-101(HPW) (black). **Part c**: FTIR spectra of (c1) MIL-101(H_2O), (c2) MIL-101(HF) and (c3) MIL-101(HPW) recorded after outgassing at 200 °C for 2 hours (blue, red, black color respectively), after adsorption of CO at room temperature (light green) and low temperature (dark green); black curves show the effect of outgassing in vacuum at low temperature. [Adapted with permission from Ref.,[95] copyright ACS 2012, and from Ref.[94] copyright RSC 2014.]

4.3 Monoglyceride synthesis

A very challenging area of heterogeneous catalysis is the synthesis of monoglycerides. Industrial monoglyceride production is currently performed at high temperature (220–250 °C) using a basic homogeneous catalyst with limited monoglyceride selectivity, owing to formation of di- and triglyceride side products and soap. The high reaction temperature bears the risk of deterioration of taste, aroma, and colour of the product. Developing a heterogeneous catalytic process at lower temperature for selective monoglyceride production is a major scientific challenge.

4.3.1 ZIF-8 catalyst

It has been discovered that nanoparticles of ZIF-8 transformed into hierarchical material through reaction with fatty acid to be a promising truly heterogeneous catalyst for monoglyceride synthesis. ZIF-8 structure resembles sodalite with 1.16 nm wide cavities connected through 0.34 nm wide windows formed by four-ring and six-ring ZnN_4 clusters (see Figure 11a).[96,97] Nanosized ZIF-8 was prepared from a synthesis solution 2.2 times more concentrated than usual.[97,98]

ZIF-8 was evaluated for esterification of oleic acid with glycerol at 150°C using a minimum of tert-butanol solvent in a mini batch reactor. Using ZIF-8 catalyst, the oleic acid conversion reached 57%, whereas in absence of catalyst conversion was limited to 10 %. Ultrastable Y zeolite[99,100] was used as a reference catalyst, as it has been reported to be an excellent solid heterogeneous catalyst for esterification reactions.[101-103] The reference zeolite catalyst reached 30% conversion. In all cases, monoglyceride was the only reaction product (100% selectivity). The ZIF-8 catalyst was recovered easily by filtration and reused in two consecutive runs without appreciable loss of activity.

Preservation of the crystal structure was concluded from PXRD and ATR FTIR spectra (see Figure 11b).

All the considered samples (fresh sample run 0 and run 1-3) show essentially many similarities in the 1800-600 cm^{-1} range. However some small differences in vibrational modes seem to increase along the runs, from 1 to 3: the new contributions at 1260, 1090, 805 cm^{-1} are not easily assigned. This means that the main framework modes remain unperturbed along the reaction runs, testifying that the main building blocks of the structure are still present.

Higher frequency Mid-IR range shows that ZIF-8 catalysts recovered in consecutive run 1, 2 and 3 are comparable to the activated ZIF-8 parent material (run 0) (see Figure 11c). IR signatures of any anomalous hydroxyl groups that may appear when a MOF is hydrolyzed are absent. The band at 2855 cm^{-1} and the shoulder at 1710 cm^{-1} on spent catalysts (Figure 11c, runs 1–3) are assigned to CH_2 and CO moieties, respectively, and attributed to entrapped residual species. IR spectra of original and hierarchical ZIF-8 samples upon CO adsorption at liquid nitrogen temperature are shown in Figure 11c (inset c2-c5). All the spectra are similar and characterized by the typical feature of CO liquefied inside pores: major spectral component around 2135 cm^{-1} tailing to lower and higher wavenumbers due to hindered rotation. The intensity of the CO absorption bands in the hierarchical samples (runs 1–3) is lower than in the parent sample, despite the generation of mesopores. This behaviour is ascribed to the lower overall porosity and the presence of entrapped species. The absence of bands around 2180 cm^{-1}, ascribable to unsaturated Zn sites and structural defects, confirms the framework integrity of the ZIF-8. This observation also explains the recyclability of the hierarchical ZIF-8 catalyst.

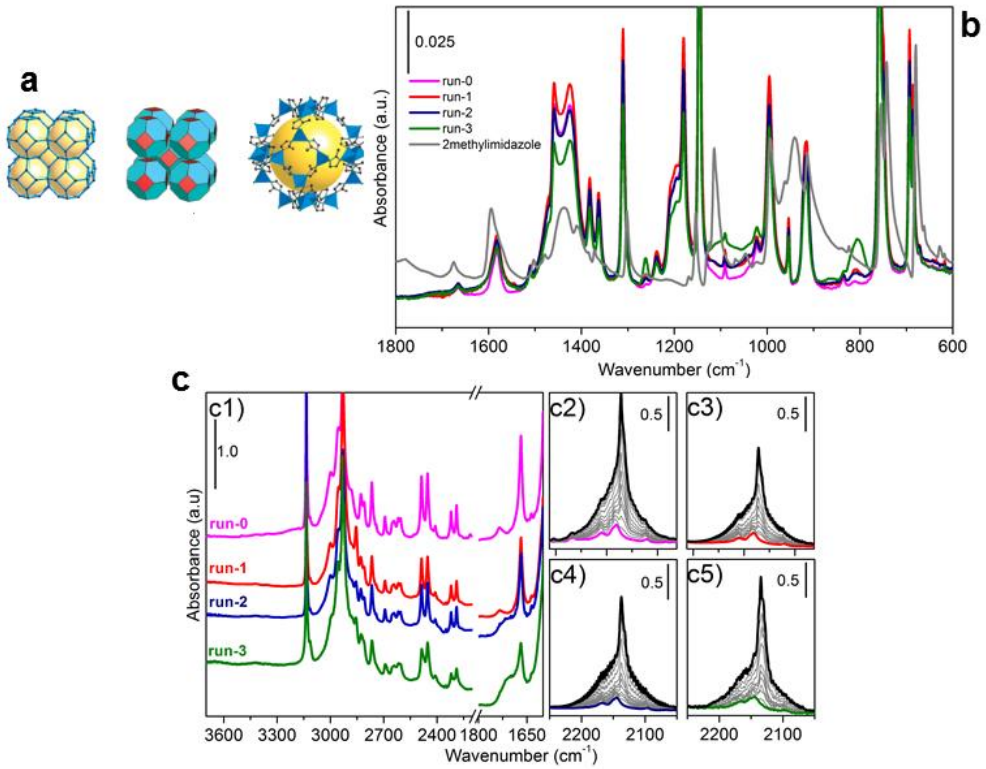

Figure 11. Part a: the single crystal X-ray structures of ZIF-8: stick diagram (left), as a tiling (center) and the largest cage shown with ZnN4 tetrahedra in blue (right); H atoms are omitted for clarity. **Part b**: FTIR spectra in ATR mode and in air of ZIF-8 catalysts and the organic linker. **Part c**: c1) FTIR normalized spectra of ZIF-8 as-synthesized (run 0) and recovered in consecutive esterification reactions (runs 1–3) recorded after activation at 573 K for 2 h. c2-c5) sequence of FTIR spectra of CO adsorption at 100 K on ZIF-8 samples from runs 0, 1, 2, and 3, respectively with background spectrum shown in color. Absorbance is normalized to pellet thickness. Self-supported pellets were prepared by pressing the ZIF-8 powder at 30 MPa. [Adapted with permission from Ref.,[97] copyright National Academy of Sciences 2006 and from Ref.,[98] copyright Wiley VCH 2013.]

In conclusion, nanosized ZIF-8 was shown to be an active and recyclable truly heterogeneous catalyst for selective monoglyceride synthesis through esterification of oleic acid with glycerol under mild reaction conditions. Fatty acid is responsible for local transformation of the framework during catalysis and creation of permanent mesopores next to the original micropores while maintaining long range framework and avoiding local defects as probed with FTIR.

4.3.2 Sn-EOF catalyst

The same reaction was tested by using Sn-EOF (Element Organic Framework) as catalyst, which enabled synthesis of monoglycerides with high selectivity and minimum leaching of tin into the reaction product. Sn-EOF is an amorphous organic framework with pore size of ca. 1 nm and thermally stable up to 200 °C (see Figure 12a). In tert-Butanol solvent Sn–EOF is catalytically active with a mixture with molar ratio of oleic acid to glycerol of 0.1:1. The oleic acid conversion reached up to 40% and 98 % monoglyceride selectivity was achieved.

The acid sites in Sn–EOF were characterized using pyridine adsorption monitored by means of FTIR spectroscopy (see Figure 12b). Sn–EOF itself has some vibrational modes overlapping with pyridine (e.g. ring modes).[104] The spectral features ascribed to pyridine appear in the difference spectra (bottom part of Figure 12b) showing positive bands due to species formed upon pyridine adsorption, and negative bands due to consumed species. Bands in the 3100–3000 cm^{-1} range were ascribed to pyridine ν(C–H) stretching modes, while the negative band at 3580 cm^{-1} was due to the consumption of some Sn–OH species, assumed to be present in defects. In the 1625–1400 cm^{-1} range, based on literature on pyridine adsorption on different materials,[105,106] all the emerging bands were attributed to pyridine interacting with a Lewis site, hydrogen-bonded (hb) or physorbed (ph). In particular the assignment can be done in the following way: 1610 8a Lewis, 1597 8a hb, 1580 8a ph or 8b hb, 1573 8b ph, 1480 19a ph or hb (probable artifact due to subtraction marked with a question mark), 1450 19b Lewis, 1443 19b hb, 1437 19b ph. It is evident that in some cases there is the superposition of some components due to the frequency closeness of the different species. In particular, for instance, for some modes the perturbation induced by Lewis sites is definitely smaller and these bands are, therefore, superimposed to those of hydrogen-bonded species. The identification of Lewis moieties is supported by comparison with IR experiments of pyridine dosed on γ-Al_2O_3 (a solid characterized by strong Lewis acid sites), where four bands, respectively at 1620 (8a), 1578 (8b), 1492 (19a), and 1450 (19b) cm^{-1}, are observed.[107] Sn-beta zeolite is known as a Sn-based Lewis acid, catalyzing a variety of green chemical reactions.[108] It was tested under the same reaction conditions and it revealed to be inactive with an oleic acid conversion of 4 % only after 20 h, even below the conversion in absence of catalyst (20 %).

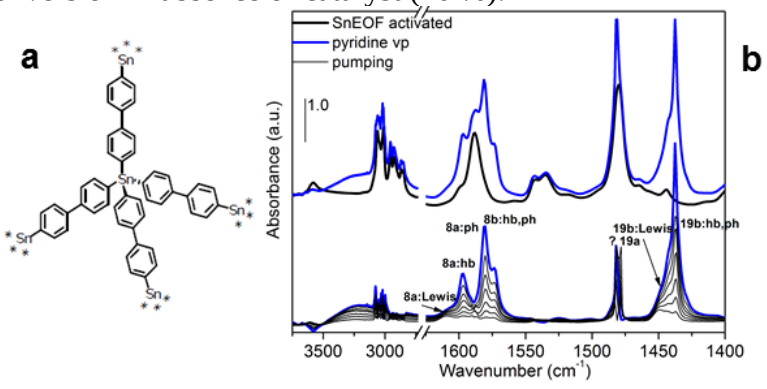

Figure 12. Part a: Sn-EOF based on Sn atoms as connectors between bifunctional organic linker molecules by direct element-carbon bond. **Part b**. Upper part: FTIR spectra of Sn–EOF activated in vacuo at 120°C for 1 night (black curve) and after pyridine vapor adsorption (blue curve). Bottom part: difference spectra (in respect to the activated sample) obtained at decreasing coverages (black curves) in respect to the highest one (blue curve). [Adapted with permission from Ref.,[104] and from Ref.,[109] copyright Springer 2013.]

5. Conclusions

In this brief review work we have underlined the potentialities of vibrational spectroscopies (infrared and Raman) in following different relevant aspects of the MOFs synthesis, functionalization (Section 2) and use, either as material for gas sorption (Section 3) or for catalysis (Section 4).

We believe that, together with autoclaves, X-ray diffractometers, volumetric and gravimetric instruments, an infrared (and possibly a Raman) spectrometer should always be present in laboratories where having the preparation and characterization of MOFs materials as core business.

References

[1] J.C. Lavalley, Infrared spectrometric studies of the surface basicity of metal oxides and zeolites using adsorbed probe molecules, *Catal. Today*, **27**, 377-401 (1996).

[2] G. Busca, Infrared studies of the reactive adsorption of organic molecules over metal oxides and of the mechanisms of their heterogeneously-catalyzed oxidation, *Catal. Today*, **27**, 457-496 (1996).

[3] A. Zecchina and C.O. Arean, Diatomic molecular probes for mid-IR studies of zeolites, *Chem. Soc. Rev.*, **25**, 187-197 (1996).

[4] H. Knozinger and S. Huber, IR spectroscopy of small and weakly interacting molecular probes for acidic and basic zeolites, *J. Chem. Soc.-Faraday Trans.*, **94**, 2047-2059 (1998).

[5] K.I. Hadjiivanov, Identification of neutral and charged NxOy surface species by IR spectroscopy, *Catal. Rev.-Sci. Eng.*, **42**, 71-144 (2000).

[6] J. Ryczkowski, IR spectroscopy in catalysis, *Catal. Today*, **68**, 263-381 (2001).

[7] A. Zecchina, D. Scarano, S. Bordiga, G. Spoto, and C. Lamberti, Surface structures of oxides and halides and their relationships to catalytic properties, *in Advances in Catalysis*, Vol. 46, 2001, pp. 265-397.

[8] K.I. Hadjiivanov and G.N. Vayssilov, Characterization of oxide surfaces and zeolites by carbon monoxide as an IR probe molecule, *in Advances in Catalysis*, B. C. Gates and H. Knozinger (Eds), Advances in Catalysis Vol. 47, Elsevier Academic Press Inc, San Diego, 2002, pp. 307-511.

[9] T. Burgi and A. Baiker, Attenuated total reflection infrared spectroscopy of solid catalysts functioning in the presence of liquid-phase reactants, *in Advances in Catalysis*, B. C. Gates and H. Knozinger (Eds), Advances in Catalysis Vol. 50, Elsevier Academic Press Inc, San Diego, 2006, pp. 227-283.

[10] C. Lamberti, E. Groppo, G. Spoto, S. Bordiga, and A. Zecchina, Infrared Spectroscopy of Transient Surface Species, *in Advances in Catalysis*, B. C. Gates and H. Knozinger (Eds), Advances in Catalysis Vol. 51, Elsevier Academic Press Inc, San Diego, 2007, pp. 1-74.

[11] G. Busca, Bases and Basic Materials in Chemical and Environmental Processes. Liquid versus Solid Basicity, *Chem. Rev.*, **110**, 2217-2249 (2010).

[12] A. Vimont, F. Thibault-Starzyk, and M. Daturi, Analysing and understanding the active site by IR spectroscopy, *Chem. Soc. Rev.*, **39**, 4928-4950 (2010).

[13] C. Lamberti, A. Zecchina, E. Groppo, and S. Bordiga, Probing the surfaces of heterogeneous catalysts by in situ IR spectroscopy, *Chem. Soc. Rev.*, **39**, 4951-5001 (2010).

[14] E. Stavitski and B.M. Weckhuysen, Infrared and Raman imaging of heterogeneous catalysts, *Chem. Soc. Rev.*, **39**, 4615-4625 (2010).

[15] F. Bonino, C. Lamberti, S. Chavan, J.G. Vitillo, and S. Bordiga, Characterization of MOFs. 1. Combined Vibrational and Electronic Spectroscopies, *in Metal Organic Frameworks as Heterogeneous Catalysts*, F.L.iX. Xamena and J. Gascon (Eds), RSC Catalysis Series Vol. 12, 2013, pp. 76-142.

[16] K. Hadjiivanov, Identification and Characterization of Surface Hydroxyl Groups by Infrared Spectroscopy, *in Advances in Catalysis*, F. C. Jentoft (Ed), Advances in Catalysis Vol. 57, Elsevier Academic Press Inc, San Diego, 2014, pp. 99-318.

[17] A. Savara and E. Weitz, Elucidation of Intermediates and Mechanisms in Heterogeneous Catalysis Using Infrared Spectroscopy, *Annu. Rev. Phys. Chem.*, **65**, 249-273 (2014).

[18] S. Bordiga, C. Lamberti, F. Bonino, A. Travert, and F. Thibault-Starzyk, Probing zeolites by vibrational spectroscopies, *Chem. Soc. Rev.*, **44**, 7262-7341 (2015).

[19] J.H. Cavka, S. Jakobsen, U. Olsbye, N. Guillou, C. Lamberti, S. Bordiga, and K.P. Lillerud, A new zirconium inorganic building brick forming metal organic frameworks with exceptional stability, *J. Am. Chem. Soc.*, **130**, 13850-13851 (2008).

[20] F. Vermoortele, B. Bueken, G. Le Bars, B. Van de Voorde, M. Vandichel, K. Houthoofd, A. Vimont, M. Daturi, M. Waroquier, V. Van Speybroeck, C. Kirschhock, and D.E. De Vos, Synthesis Modulation as a Tool To Increase the Catalytic Activity of Metal-Organic Frameworks: The Unique Case of UiO-66(Zr), *J. Am. Chem. Soc.*, **135**, 11465-11468 (2013).

[21] H. Wu, Y.S. Chua, V. Krungleviciute, M. Tyagi, P. Chen, T. Yildirim, and W. Zhou, Unusual and Highly Tunable Missing-Linker Defects in Zirconium Metal-Organic Framework UiO-66 and Their Important Effects on Gas Adsorption, *J. Am. Chem. Soc.*, **135**, 10525-10532 (2013).
[22] G.C. Shearer, S. Chavan, J. Ethiraj, J.G. Vitillo, S. Svelle, U. Olsbye, C. Lamberti, S. Bordiga, and K.P. Lillerud, Tuned to Perfection: Ironing Out the Defects in Metal-Organic Framework UiO-66, *Chem. Mater.*, **26**, 4068-4071 (2014).
[23] P.S. Barcia, D. Guimaraes, P.A.P. Mendes, J.A.C. Silva, V. Guillerm, H. Chevreau, C. Serre, and A.E. Rodrigues, Reverse shape selectivity in the adsorption of hexane and xylene isomers in MOF UiO-66, *Micropor. Mesopor. Mat.*, **139**, 67-73 (2011).
[24] It is out of the scope of the present work entering into the details of the simulation of IR and Raman spectra of MOFs. However, it is worth noting that the accurate simulation of vibrational spectra for solid state is nowadays feasible by using ab initio methods. Several computational tools are available to calculate IR and Raman intensities. A non exhaustive list of softwares that includes both commercial and open source codes, follows: VASP (https://www.vasp.at), Quantum Espresso (http://www.quantum-espresso.org), ABINIT (http://www.abinit.org/), CASTEP (http://www.castep.org/) and CRYSTAL (http://www.crystal.unito.it/index.php). In particular, the latter has been successfully employed to simulate the IR and Raman spectra of several MOFs including MOF-5, UiO-66, UiO-67, UiO-66-NH_2, Ni-bpz, Ni-bpb, CPO-27-Ni.
[25] R. Dovesi, R. Orlando, A. Erba, C.M. Zicovich-Wilson, B. Civalleri, S. Casassa, L. Maschio, M. Ferrabone, M. De La Pierre, P. D'Arco, Y. Noel, M. Causà, M. Rerat, and B. Kirtman, *Int. J. Quantum Chem.*, **114**, 1287-1317 (2014).
[26] R. Dovesi, V.R. Saunders, C. Roetti, R. Orlando, C.M. Zicovich-Wilson, F. Pascale, B. Civalleri, K. Doll, N.M. Harrison, I.J. Bush, P. D'Arco, M. Llunell, M. Causà, and Y. Noël, CRYSTAL14 User's Manual (University of Torino Torino, 2014).
[27] V. Guillerm, F. Ragon, M. Dan-Hardi, T. Devic, M. Vishnuvarthan, B. Campo, A. Vimont, G. Clet, Q. Yang, G. Maurin, G. Ferey, A. Vittadini, S. Gross, and C. Serre, A Series of Isoreticular, Highly Stable, Porous Zirconium Oxide Based Metal-Organic Frameworks, *Angew. Chem.-Int. Edit.*, **51**, 9267-9271 (2012).
[28] S. Chavan, J.G. Vitillo, D. Gianolio, O. Zavorotynska, B. Civalleri, S. Jakobsen, M.H. Nilsen, L. Valenzano, C. Lamberti, K.P. Lillerud, and S. Bordiga, H_2 storage in isostructural UiO-67 and UiO-66 MOFs, *Phys. Chem. Chem. Phys.*, **14**, 1614-1626 (2012).
[29] S.M. Chavan, G.C. Shearer, S. Svelle, U. Olsbye, F. Bonino, J. Ethiraj, K.P. Lillerud, and S. Bordiga, Synthesis and Characterization of Amine-Functionalized Mixed-Ligand Metal-Organic Frameworks of UiO-66 Topology, *Inorg. Chem.*, **53**, 9509-9515 (2014).
[30] J. Ethiraj, E. Albanese, B. Civalleri, J.G. Vitillo, F. Bonino, S. Chavan, G.C. Shearer, K.P. Lillerud, and S. Bordiga, Carbon Dioxide Adsorption in Amine-Functionalized Mixed-Ligand Metal-Organic Frameworks of UiO-66 Topology, *ChemSusChem*, **7**, 3382-3388 (2014).
[31] L. Valenzano, B. Civalleri, S. Chavan, S. Bordiga, M.H. Nilsen, S. Jakobsen, K.P. Lillerud, and C. Lamberti, Disclosing the Complex Structure of UiO-66 Metal Organic Framework: A Synergic Combination of Experiment and Theory, *Chem. Mater.*, **23**, 1700-1718 (2011).
[32] M. Kandiah, M.H. Nilsen, S. Usseglio, S. Jakobsen, U. Olsbye, M. Tilset, C. Larabi, E.A. Quadrelli, F. Bonino, and K.P. Lillerud, Synthesis and Stability of Tagged UiO-66 Zr-MOFs, *Chem. Mater.*, **22**, 6632-6640 (2010).
[33] U. Ravon, G. Chaplais, C. Chizallet, B. Seyyedi, F. Bonino, S. Bordiga, N. Bats, and D. Farrusseng, Investigation of Acid Centers in MIL-53(Al, Ga) for Bronsted-Type Catalysis: In Situ FTIR and Ab Initio Molecular Modeling, *ChemCatChem*, **2**, 1235-1238 (2010).
[34] L. Mino, V. Colombo, J.G. Vitillo, C. Lamberti, S. Bordiga, E. Gallo, P. Glatzel, A. Maspero, and S. Galli, Spectroscopic and adsorptive studies of a thermally robust pyrazolato-based PCP, *Dalton Trans.*, **41**, 4012-4019 (2012).
[35] G.C. Shearer, V. Colombo, S. Chavan, E. Albanese, B. Civalleri, A. Maspero, and S. Bordiga, Stability vs. reactivity: understanding the adsorption properties of $Ni_3(BTP)_2$ by experimental and computational methods, *Dalton Trans.*, **42**, 6450-6458 (2013).
[36] S. Chavan, F. Bonino, J.G. Vitillo, E. Groppo, C. Lamberti, P.D.C. Dietzel, A. Zecchina, and S. Bordiga, Response of CPO-27-Ni towards CO, N_2 and C_2H_4, *Phys. Chem. Chem. Phys.*, **11**, 9811-9822 (2009).
[37] S. Chavan, J.G. Vitillo, E. Groppo, F. Bonino, C. Lamberti, P.D.C. Dietzel, and S. Bordiga, CO Adsorption on CPO-27-Ni Coordination Polymer: Spectroscopic Features and Interaction Energy, *J. Phys. Chem. C*, **113**, 3292-3299 (2009).
[38] F. Bonino, S. Chavan, J.G. Vitillo, E. Groppo, G. Agostini, C. Lamberti, P.D.C. Dietzel, C. Prestipino, and S. Bordiga, Local structure of CPO-27-Ni metallorganic framework upon dehydration and coordination of NO, *Chem. Mater.*, **20**, 4957-4968 (2008).
[39] C. Prestipino, L. Regli, J.G. Vitillo, F. Bonino, A. Damin, C. Lamberti, A. Zecchina, P.L. Solari, K.O. Kongshaug, and S. Bordiga, Local structure of framework Cu(II) in HKUST-1 metallorganic framework: Spectroscopic characterization upon activation and interaction with adsorbates, *Chem. Mater.*, **18**, 1337-1346 (2006).

[40] C.O. Arean, O.V. Manoilova, G.T. Palomino, M.R. Delgado, A.A. Tsyganenko, B. Bonelli, and E. Garrone, Variable-temperature infrared spectroscopy: An access to adsorption thermodynamics of weakly interacting systems, *Phys. Chem. Chem. Phys.*, **4**, 5713-5715 (2002).
[41] G. Spoto, E.N. Gribov, G. Ricchiardi, A. Damin, D. Scarano, S. Bordiga, C. Lamberti, and A. Zecchina, Carbon Monoxide MgO from Dispersed Solids to Single Crystals: A Review and New Advances, *Prog. Surf. Sci.*, **76**, 71-146 (2004).
[42] J.G. Vitillo, L. Regli, S. Chavan, G. Ricchiardi, G. Spoto, P.D.C. Dietzel, S. Bordiga, and A. Zecchina, Role of exposed metal sites in hydrogen storage in MOFs, *J. Am. Chem. Soc.*, **130**, 8386-8396 (2008).
[43] L. Valenzano, B. Civalleri, S. Chavan, G.T. Palomino, C.O. Arean, and S. Bordiga, Computational and Experimental Studies on the Adsorption of CO, N_2, and CO_2 on Mg-MOF-74, *J. Phys. Chem. C*, **114**, 11185-11191 (2010).
[44] L. Valenzano, J.G. Vitillo, S. Chavan, B. Civalleri, F. Bonino, S. Bordiga, and C. Lamberti, Structure-activity relationships of simple molecules adsorbed on CPO-27-Ni metal-organic framework: In situ experiments vs. theory, *Catal. Today*, **182**, 67-79 (2012).
[45] E.D. Bloch, M.R. Hudson, J.A. Mason, S. Chavan, V. Crocella, J.D. Howe, K. Lee, A.L. Dzubak, W.L. Queen, J.M. Zadrozny, S.J. Geier, L.-C. Lin, L. Gagliardi, B. Smit, J.B. Neaton, S. Bordiga, C.M. Brown, and J.R. Long, Reversible CO Binding Enables Tunable CO/H_2 and CO/N_2 Separations in Metal-Organic Frameworks with Exposed Divalent Metal Cations, *J. Am. Chem. Soc.*, **136**, 10752-10761 (2014).
[46] K. Sumida, D. Stueck, L. Mino, J.-D. Chai, E.D. Bloch, O. Zavorotynska, L.J. Murray, M. Dinca, S. Chavan, S. Bordiga, M. Head-Gordon, and J.R. Long, Impact of Metal and Anion Substitutions on the Hydrogen Storage Properties of M-BTT Metal-Organic Frameworks, *J. Am. Chem. Soc.*, **135**, 1083-1091 (2013).
[47] S.M. Chavan, O. Zavorotynska, C. Lamberti, and S. Bordiga, H_2 interaction with divalent cations in isostructural MOFs: a key study for variable temperature infrared spectroscopy, *Dalton Trans.*, **42**, 12586-12595 (2013).
[48] N.L. Rosi, J. Kim, M. Eddaoudi, B.L. Chen, M. O'Keeffe, and O.M. Yaghi, Rod packings and metal-organic frameworks constructed from rod-shaped secondary building units, *J. Am. Chem. Soc.*, **127**, 1504-1518 (2005).
[49] P.D.C. Dietzel, B. Panella, M. Hirscher, R. Blom, and H. Fjellvag, Hydrogen adsorption in a nickel based coordination polymer with open metal sites in the cylindrical cavities of the desolvated framework, *Chem. Commun.*, 959-961 (2006).
[50] A. Zecchina, S. Bordiga, C. Lamberti, G. Spoto, L. Carnelli, and C. Otero Aréan, Low-Temperature Fourier-Transform Infrared Study of the Interaction of CO with Cations in Alkali-Metal Exchanged ZSM-5 Zeolites, *J. Phys. Chem.*, **98**, 9577-9582 (1994).
[51] C. Lamberti, S. Bordiga, F. Geobaldo, A. Zecchina, and C. Otero Aréan, Stretching Frequencies of Cation CO Adducts in Alkali-Metal Exchanged Zeolites - an Elementary Electrostatic Approach, *J. Chem. Phys.*, **103**, 3158-3165 (1995).
[52] S. Bordiga, C. Lamberti, F. Geobaldo, A. Zecchina, G. Turnes Palomino, and C. Otero Aréan, Fourier-Transform Infrared Study of CO Adsorbed at 77-K on H-Mordenite and Alkali-Metal-Exchanged Mordenites, *Langmuir*, **11**, 527-533 (1995).
[53] S. Bordiga, G.T. Palomino, D. Arduino, C. Lamberti, A. Zecchina, and C.O. Arean, Well defined carbonyl complexes in Ag^+- and Cu^+-exchanged ZSM-5 zeolite: a comparison with homogeneous counterparts, *J. Mol. Catal. A-Chem.*, **146**, 97-106 (1999).
[54] A.J. Lupinetti, S.H. Strauss, and G. Frenking, Nonclassical metal carbonyls, *in Progress in Inorganic Chemistry*, K. D. Karlin (Ed), Progress in Inorganic Chemistry Vol. 49, JOHN WILEY & SONS INC, New York, 2001, pp. 1-112.
[55] V. Bolis, A. Barbaglia, S. Bordiga, C. Lamberti, and A. Zecchina, Heterogeneous nonclassical carbonyls stabilized in Cu(I)- and Ag(I)-ZSM-5 zeolites: Thermodynamic and spectroscopic features, *J. Phys. Chem. B*, **108**, 9970-9983 (2004).
[56] E. Groppo, C. Lamberti, S. Bordiga, G. Spoto, and A. Zecchina, The structure of active centers and the ethylene polymerization mechanism on the Cr/SiO_2 catalyst: a frontier for the characterization methods, *Chem. Rev.*, **105**, 115-183 (2005).
[57] P. Li, Y. Xiang, V.H. Grassian, and S.C. Larsen, CO adsorption as a probe of acid sites and the electric field in alkaline earth exchanged zeolite beta using FT-IR and ab initio quantum calculations, *J. Phys. Chem. B*, **103**, 5058-5062 (1999).
[58] K. Hadjiivanov, H. Knozinger, and M. Mihaylov, FTIR study of CO adsorption on Ni-ZSM-5, *J. Phys. Chem. B*, **106**, 2618-2624 (2002).
[59] A. Penkova, S. Dzwigaj, R. Kefirov, K. Hadjiivanov, and M. Che, Effect of the preparation method on the state of nickel ions in BEA zeolites. A study by Fourier transform infrared spectroscopy of adsorbed CO and NO, temperature-programmed reduction, and X-ray diffraction, *J. Phys. Chem. C*, **111**, 8623-8631 (2007).
[60] M. Mihaylov, E. Ivanova, K. Chakarova, P. Novachka, and K. Hadjiivanov, Reduced iron sites in Fe-BEA and Fe-ZSM-5 zeolites: FTIR study of CO adsorption and $^{12}C^{16}O$-$^{13}C^{18}O$ co-adsorption, *Appl. Catal. A-Gen.*, **391**, 3-10 (2011).

[61] K. Hadjiivanov, B. Tsyntsarski, T. Venkov, D. Klissurski, M. Daturi, J. Saussey, and J.C. Lavalley, FTIR spectroscopic study of CO adsorption on Co-ZSM-5: Evidence of formation of $Co^{+}(CO)_4$ species, *Phys. Chem. Chem. Phys.*, **5**, 1695-1702 (2003).
[62] K. Otsuka, J. Manda, and A. Morikaw, Location of Zn^{2+} ions in Zn-Y zeolites and the SO2-induced activities in the isomerization of cis-but-2-ene, *J. Chem. Soc., Faraday Trans. 1*, **77**, 2429-2438 (1981).
[63] D. Scarano, G. Spoto, S. Bordiga, S. Coluccia, and A. Zecchina, CO adsorption at 77 K on CoO/MgO and NiO/MgO solid-solutions - A Fourier-transform infrared study, *J. Chem. Soc.-Faraday Trans.*, **88**, 291-296 (1992).
[64] D. Scarano, G. Ricchiardi, S. Bordiga, P. Galletto, C. Lamberti, G. Spoto, and A. Zecchina, Modelling of a-Cr_2O_3 and ZnO crystal morphology and its relation to the vibrational spectra of adsorbed CO, *Faraday Discuss.*, **105**, 119-138 (1996).
[65] D. Scarano, P. Galletto, C. Lamberti, R. DeFranceschi, and A. Zecchina, Morphology and CO adsorptive properties of CuCl polycrystalline films: a SEM and FTIR study, *Surf. Sci.*, **387**, 236-242 (1997).
[66] D. Scarano, S. Bordiga, C. Lamberti, G. Spoto, G. Ricchiardi, A. Zecchina, and C.O. Arean, FTIR study of the interaction of CO with pure and silica-supported copper(I) oxide, *Surf. Sci.*, **411**, 272-285 (1998).
[67] D. Scarano, G. Spoto, S. Bordiga, A. Zecchina, and C. Lamberti, Lateral interactions in CO adlayers on prismatic ZnO faces - a FTIR and hrtem study, *Surf. Sci.*, **276**, 281-298 (1992).
[68] S. Bordiga, E. Escalona Platero, C. Otero Areán, C. Lamberti, and A. Zecchina, Low temperature CO adsorption on Na-ZSM-5 Zeolites - an FTIR investigation, *J. Catal.*, **137**, 179-185 (1992).
[69] S. Bordiga, D. Scarano, G. Spoto, A. Zecchina, C. Lamberti, and C.O. Arean, Infrared study of carbon-monoxide adsorption at 77-K on faujasites and ZSM-5 zeolites, *Vib. Spectrosc.*, **5**, 69-74 (1993).
[70] G. Ramis, G. Busca, and V. Lorenzelli, Low-temperature CO_2 adsorption on metal-oxides - spectroscopic characterization of some weakly adsorbed species, *Mater. Chem. Phys.*, **29**, 425-435 (1991).
[71] E. Garrone, B. Bonelli, C. Lamberti, B. Civalleri, M. Rocchia, P. Roy, and C.O. Arean, Coupling of framework modes and adsorbate vibrations for CO_2 molecularly adsorbed on alkali ZSM-5 zeolites: Mid- and far-infrared spectroscopy and ab initio modeling, *J. Chem. Phys.*, **117**, 10274-10282 (2002).
[72] F. Xamena and A. Zecchina, FTIR spectroscopy of carbon dioxide adsorbed on sodium- and magnesium-exchanged ETS-10 molecular sieves, *Phys. Chem. Chem. Phys.*, **4**, 1978-1982 (2002).
[73] D.H. Gibson, Carbon dioxide coordination chemistry: metal complexes and surface-bound species. What relationships?, *Coord. Chem. Rev.*, **185-186**, 335-355 (1999).
[74] S. Bordiga, L. Regli, F. Bonino, E. Groppo, C. Lamberti, B. Xiao, P.S. Wheatley, R.E. Morris, and A. Zecchina, Adsorption properties of HKUST-1 toward hydrogen and other small molecules monitored by IR, *Phys. Chem. Chem. Phys.*, **9**, 2676-2685 (2007).
[75] P.D.C. Dietzel, R.E. Johnsen, H. Fjellvag, S. Bordiga, E. Groppo, S. Chavan, and R. Blom, Adsorption properties and structure of CO_2 adsorbed on open coordination sites of metal-organic framework Ni(2)(dhtp) from gas adsorption, IR spectroscopy and X-ray diffraction, *Chem. Commun.*, 5125-5127 (2008).
[76] T. Devic, F. Salles, S. Bourrelly, B. Moulin, G. Maurin, P. Horcajada, C. Serre, A. Vimont, J.-C. Lavalley, H. Leclerc, G. Clet, M. Daturi, P.L. Llewellyn, Y. Filinchuk, and G. Ferey, Effect of the organic functionalization of flexible MOFs on the adsorption of CO_2, *J. Mater. Chem.*, **22**, 10266-10273 (2012).
[77] C. Serre, S. Bourrelly, A. Vimont, N.A. Ramsahye, G. Maurin, P.L. Llewellyn, M. Daturi, Y. Filinchuk, O. Leynaud, P. Barnes, and G. Ferey, An explanation for the very large breathing effect of a metal-organic framework during CO_2 adsorption, *Adv. Mater.*, **19**, 2246–2251 (2007).
[78] S. Chavan, PhD Thesis "Characterization of Metal-Organic Frameworks for gas storage and catalysis applications", 2010.
[79] W.L. Queen, C.M. Brown, D.K. Britt, P. Zajdel, M.R. Hudson, and O.M. Yaghi, Site-Specific CO_2 Adsorption and Zero Thermal Expansion in an An isotropic Pore Network, *J. Phys. Chem. C*, **115**, 24915-24919 (2011).
[80] W.L. Queen, M.R. Hudson, E.D. Bloch, J.A. Mason, M.I. Gonzalez, J.S. Lee, D. Gygi, J.D. Howe, K. Lee, T.A. Darwish, M. James, V.K. Peterson, S.J. Teat, B. Smit, J.B. Neaton, J.R. Long, and C.M. Brown, Comprehensive study of carbon dioxide adsorption in the metal-organic frameworks M_2(dobdc) (M = Mg, Mn, Fe, Co, Ni, Cu, Zn), *Chem. Sci.*, **5**, 4569-4581 (2014).
[81] S.R. Caskey, A.G. Wong-Foy, and A.J. Matzger, Dramatic tuning of carbon dioxide uptake via metal substitution in a coordination polymer with cylindrical pores, *J. Am. Chem. Soc.*, **130**, 10870-10871 (2008).
[82] P.D.C. Dietzel, V. Besikiotis, and R. Blom, Application of metal-organic frameworks with coordinatively unsaturated metal sites in storage and separation of methane and carbon dioxide, *J. Mater. Chem.*, **19**, 7362-7370 (2009).
[83] D. Yu, A.O. Yazaydin, J.R. Lane, P.D.C. Dietzel, and R.Q. Snurr, A combined experimental and quantum chemical study of CO_2 adsorption in the metal-organic framework CPO-27 with different metals, *Chem. Sci.*, **4**, 3544-3556 (2013).

[84] C. Serre, F. Millange, C. Thouvenot, M. Nogues, G. Marsolier, D. Louer, and G. Ferey, Very large breathing effect in the first nanoporous chromium(III)-based solids: MIL-53 or Cr-^{III}(OH)center·{O_2C-C_6H_4-CO_2}·{HO_2C-C_6H_4-CO_2H}$_x$·H_2O_y, *J. Am. Chem. Soc.*, **124**, 13519-13526 (2002).
[85] T. Loiseau, C. Serre, C. Huguenard, G. Fink, F. Taulelle, M. Henry, T. Bataille, and G. Ferey, A rationale for the large breathing of the porous aluminum terephthalate (MIL-53) upon hydration, *Chem.-Eur. J.* , **10**, 1373-1382 (2004).
[86] S. Bourrelly, P.L. Llewellyn, C. Serre, F. Millange, T. Loiseau, and G. Ferey, Different adsorption behaviors of methane and carbon dioxide in the isotypic nanoporous metal terephthalates MIL-53 and MIL-47, *J. Am. Chem. Soc.*, **127**, 13519-13521 (2005).
[87] T.M. McDonald, J.A. Mason, X.Q. Kong, E.D. Bloch, D. Gygi, A. Dani, V. Crocella, F. Giordanino, S.O. Odoh, W.S. Drisdell, B. Vlaisavljevich, A.L. Dzubak, R. Poloni, S.K. Schnell, N. Planas, K. Lee, T. Pascal, L.W.F. Wan, D. Prendergast, J.B. Neaton, B. Smit, J.B. Kortright, L. Gagliardi, S. Bordiga, J.A. Reimer, and J.R. Long, Cooperative insertion of CO_2 in diamine-appended metal-organic frameworks, *Nature*, **519**, 303-308 (2015).
[88] A. Demessence, D.M. D'Alessandro, M.L. Foo, and J.R. Long, Strong CO_2 Binding in a Water-Stable, Triazolate-Bridged Metal-Organic Framework Functionalized with Ethylenediamine, *J. Am. Chem. Soc.*, **131**, 8784-8786 (2009).
[89] T.M. McDonald, D.M. D'Alessandro, R. Krishna, and J.R. Long, Enhanced carbon dioxide capture upon incorporation of N,N '-dimethylethylenediamine in the metal-organic framework CuBTTri, *Chem. Sci.*, **2**, 2022-2028 (2011).
[90] T.M. McDonald, W.R. Lee, J.A. Mason, B.M. Wiers, C.S. Hong, and J.R. Long, Capture of Carbon Dioxide from Air and Flue Gas in the Alkylamine-Appended Metal-Organic Framework mmen-Mg_2(dobpdc), *J. Am. Chem. Soc.*, **134**, 7056-7065 (2012).
[91] D.J. Xiao, E.D. Bloch, J.A. Mason, W.L. Queen, M.R. Hudson, N. Planas, J. Borycz, A.L. Dzubak, P. Verma, K. Lee, F. Bonino, V. Crocella, J. Yano, S. Bordiga, D.G. Truhlar, L. Gagliardi, C.M. Brown, and J.R. Long, Oxidation of ethane to ethanol by N_2O in a metal-organic framework with coordinatively unsaturated iron(II) sites, *Nat. Chem.*, **6**, 590-595 (2014).
[92] M. Rivallan, G. Ricchiardi, S. Bordiga, and A. Zecchina, Adsorption and reactivity of nitrogen oxides (NO_2, NO, N_2O) on Fe-zeolites, *J. Catal.*, **264**, 104-116 (2009).
[93] G. Ferey, C. Mellot-Draznieks, C. Serre, F. Millange, J. Dutour, S. Surble, and I. Margiolaki, A chromium terephthalate-based solid with unusually large pore volumes and surface area, *Science*, **309**, 2040-2042 (2005).
[94] L.H. Wee, F. Bonino, C. Lamberti, S. Bordiga, and J.A. Martens, Cr-MIL-101 encapsulated Keggin phosphotungstic acid as active nanomaterial for catalysing the alcoholysis of styrene oxide, *Green Chem.*, **16**, 1351-1357 (2014).
[95] L. Bromberg, Y. Diao, H. Wu, S.A. Speakman, and T.A. Hatton, Chromium(III) Terephthalate Metal Organic Framework (MIL-101): HF-Free Synthesis, Structure, Polyoxometalate Composites, and Catalytic Properties, *Chem. Mater.*, **24**, 1664-1675 (2012).
[96] X.C. Huang, Y.Y. Lin, J.P. Zhang, and X.M. Chen, Ligand-directed strategy for zeolite-type metal-organic frameworks: Zinc(II) imidazolates with unusual zeolitic topologies, *Angew. Chem.-Int. Edit.*, **45**, 1557-1559 (2006).
[97] K.S. Park, Z. Ni, A.P. Cote, J.Y. Choi, R. Huang, F.J. Uribe-Romo, H.K. Chae, M. O'Keeffe, and O.M. Yaghi, Exceptional chemical and thermal stability of zeolitic imidazolate frameworks, *Proc. Natl. Acad. Sci. U. S. A.* , **103**, 10186-10191 (2006).
[98] L.H. Wee, T. Lescouet, J. Ethiraj, F. Bonino, R. Vidruk, E. Garrier, D. Packet, S. Bordiga, D. Farrusseng, M. Herskowitz, and J.A. Martens, Hierarchical Zeolitic Imidazolate Framework-8 Catalyst for Monoglyceride Synthesis, *ChemCatChem*, **5**, 3562-3566 (2013).
[99] A. Corma, Inorganic solid acids and their use in acid-catalyzed hydrocarbon reactions, *Chem. Rev.*, **95**, 559-614 (1995).
[100] G. Agostini, C. Lamberti, L. Palin, M. Milanesio, N. Danilina, B. Xu, M. Janousch, and J.A. van Bokhoven, In Situ XAS and XRPD Parametric Rietveld Refinement To Understand Dealumination of Y Zeolite Catalyst, *J. Am. Chem. Soc.*, **132**, 667-678 (2010).
[101] M.A. Wegman, J.M. Elzinga, E. Neeleman, F. van Rantwijk, and R.A. Sheldon, Salt-free esterification of alpha-amino acids catalysed by zeolite H-USY, *Green Chem.*, **3**, 61-64 (2001).
[102] T.A. Peters, N.E. Benes, A. Holmen, and J.T.F. Keurentjes, Comparison of commercial solid acid catalysts for the esterification of acetic acid with butanol, *Appl. Catal. A-Gen.*, **297**, 182-188 (2006).
[103] P. Ferreira, I.M. Fonseca, A.M. Ramos, J. Vital, and J.E. Castanheiro, Esterification of glycerol with acetic acid over dodecamolybdophosphoric acid encaged in USY zeolite, *Catal. Commun.*, **10**, 481-484 (2009).
[104] J. Fritsch, M. Rose, P. Wollmann, W. Boehlmann, and S. Kaskel, New Element Organic Frameworks Based on Sn, Sb, and Bi, with Permanent Porosity and High Catalytic Activity, *Materials*, **3**, 2447-2462 (2010).
[105] F. Bonino, A. Damin, S. Bordiga, C. Lamberti, and A. Zecchina, Interaction of CD_3CN and pyridine with the Ti(IV) centers of TS-1 catalysts: a spectroscopic and computational study, *Langmuir*, **19**, 2155-2161 (2003).

[106] R. Buzzoni, S. Bordiga, G. Ricchiardi, C. Lamberti, A. Zecchina, and G. Bellussi, Interaction of pyridine with acidic (H-ZSM5, H-beta, H-MORD zeolites) and superacidic (H-Nafion membrane) systems: An IR investigation, *Langmuir*, **12**, 930-940 (1996).
[107] C. Morterra and G. Magnacca, A case study: Surface chemistry and surface structure of catalytic aluminas, as studied by vibrational spectroscopy of adsorbed species, *Catal. Today*, **27**, 497-532 (1996).
[108] A. Corma, L.T. Nemeth, M. Renz, and S. Valencia, Sn-zeolite beta as a heterogeneous chemoselective catalyst for Baeyer-Villiger oxidations, *Nature*, **412**, 423-425 (2001).
[109] L.H. Wee, T. Lescouet, J. Fritsch, F. Bonino, M. Rose, Z. Sui, E. Garrier, D. Packet, S. Bordiga, S. Kaskel, M. Herskowitz, D. Farrusseng, and J.A. Martens, Synthesis of Monoglycerides by Esterification of Oleic Acid with Glycerol in Heterogeneous Catalytic Process Using Tin-Organic Framework Catalyst, *Catal. Lett.*, **143**, 356-363 (2013).